INSTITUT DE FRANCE
Académie des sciences

Comptes Rendus

Physique

Jean-Paul Pouget

Basic aspects of the metal–insulator transition in vanadium dioxide VO_2: a critical review

Volume 22, issue 1 (2021), p. 37-87

Published online: 11 June 2021

https://doi.org/10.5802/crphys.74

Les Comptes Rendus. Physique *sont membres du*
Centre Mersenne pour l'édition scientifique ouverte
www.centre-mersenne.org
e-ISSN : 1878-1535

Comptes Rendus
Physique
2021, 22, nº 1, p. 37-87
https://doi.org/10.5802/crphys.74

Research article / *Article de recherche*

Basic aspects of the metal–insulator transition in vanadium dioxide VO_2: a critical review

Aspects principaux de la transition métal–isolant du dioxyde de vanadium VO_2 : une revue critique

Jean-Paul Pouget [a]

[a] Laboratoire de physique des solides, CNRS UMR 8502, Université Paris-Sud, Université Paris-Saclay, 91405 Orsay, France
E-mail: jean-paul.pouget@u-psud.fr

Abstract. Vanadium dioxide exhibits a first order metal to insulator transition (MIT) at 340 K (T_{MI}) from a rutile (R) structure to a monoclinic (M_1) structure. The mechanism of this transition interpreted as due either to a Peierls instability or to a Mott–Hubbard instability is controversial since half a century. However, in the last twenty years the study of chemical and physical properties of VO_2 and of its alloys, benefits of a renewed interest due to possible applications coming from the realization of devices made of thin films. We describe in this review the structural, electronic and magnetic properties of the different metallic (R) and insulating (M_1, T, M_2) phases of VO_2, of its solid solutions and under constraint. We present in a synthetic manner the various phase diagrams and their symmetry analysis. This work allows us to revisit older interpretation and to emphasize in particular the combined role of electron–electron interactions in the various phase of VO_2 and of structural fluctuations in the MIT mechanism. In this framework we show that the phase transition is surprisingly announced by anisotropic one-dimensional (1D) structural fluctuations revealing chain like correlations between the V due to an incipient instability of the rutile structure. This leads to an unexpected critical dynamics of the order–disorder (or relaxation) type. We describe how the two-dimensional (2D) coupling between these 1D fluctuations, locally forming uniform V^{4+} zig-zag chains and V–V pairs, stabilizes the M_2 and M_1 insulating phases. These phases exhibit a 1D electronic anisotropy where substantial electron–electron correlations conduct to a spin–charge decoupling. The spin-Peierls ground state of M_1 is analyzed via a mechanism of dimerization, in the T phase, of the spin 1/2 V^{4+} zig-zag Heisenberg chains formed in the M_2 phase. This review summarizes in a critical manner the main results of the large literature on fundamental aspects of the MIT of VO_2. It is completed by unpublished old results. Interpretations are also placed in a large conceptual frame which is also relevant to interpret physical properties of other classes of materials.

Résumé. Le dioxyde de vanadium présente une transition métal–isolant (TMI) du premier ordre à 340 K (=T_{MI}) d'une structure rutile (R) à une structure monoclinique (M_1). Le mécanisme de cette transition interprétée comme étant due soit à une instabilité de Peierls soit à une instabilité de Mott–Hubbard reste très controversé depuis près d'un demi-siècle. Cependant depuis une vingtaine d'années l'étude des propriétés chimiques et physiques de VO_2 et de ses alliages suscite un renouveau d'intérêt par la possibilité d'applications provenant de l'obtention de dispositifs s'appuyant sur la réalisation de films minces. Nous décrivons dans cette revue les propriétés structurales, électroniques et magnétiques des différentes phases métallique

(R) et isolantes (M_1, T et M_2) de VO_2, de ses solutions solides et des modifications sous contrainte. Nous présentons de façon synthétique les divers diagrammes de phase et leur analyse par symétrie. Ce travail conduit à relativiser certaines interprétations du passé et à souligner en particulier le rôle particulièrement important des interactions électron–électron dans les différentes phases de VO_2 et des fluctuations structurales dans le mécanisme de la TMI. Dans ce cadre nous montrons que la transition de phase est annoncée de façon surprenante par des corrélations structurales d'anisotropie unidimensionnelle (1D) révélant un ordre local en chaine du V issu d'une instabilité sous-jacente de la structure rutile. A celles-ci correspond une dynamique critique inattendue de type relaxation (ou ordre-désordre). Nous décrivons comment le couplage bidimensionnel (2D) de ces fluctuations 1D forme localement des chaines zig-zag de V^{4+} et des paires V–V, conduisant aux phases isolantes M_2 et M_1. Ces phases présentent une forte anisotropie électronique avec de substantielles corrélations électron–électron conduisant à un découplage spin–charge. Le fondamental de type spin-Peierls de la phase M_1 est analysé à partir d'un mécanisme de dimérisation, en phase T, des chaines d'Heisenberg de spin 1/2 formées par les zig-zags de V^{4+} dans la phase M_2. Cette revue résume de façon critique les résultats principaux de l'abondante littérature concernant les aspects fondamentaux de la TMI de VO_2. Elle est complétée par d'anciens résultats jamais publiés. Les interprétations proposées se placent dans un cadre conceptuel relativement large se révélant pertinent pour l'interprétation des propriétés physiques d'autres classes de matériaux.

Keywords. Vanadium dioxide, Metal–insulator transition, Mott–Hubbard charge localization, Spin-Peierls and Peierls transitions,Chain-like structural instability, Electron–phonon coupling.

Mots-clés. Dioxyde de vanadium, Transition métal–isolant, Localisation de charge de Mott–Hubbard, Transitions de Peierls et de spin-Peierls, Instabilités structurales corrélées à une dimension, Couplage électron–phonon.

Manuscript received 28th November 2020, revised 25th February 2021 and 16th April 2021, accepted 20th April 2021.

Contents

1. Historical introduction

The study of the metal–insulator transition (MIT) has remained one of the most important field of research in solid state physics for more than half a century. The reason is that MIT raised unsolved fundamental questions and nowadays has become the subject of important applied research. Relevant mechanisms of MIT, which were already exposed in the 1970's, rely either on a modification of the electronic structure due to crystalline symmetry change, or electron–electron correlations, anti-ferromagnetism and the Mott transition [1, 2]. The former class of mechanisms considers non interacting electrons in a lattice submitted to a structural distortion whose associated electronic potential opens a gap at the Fermi level [3]. These MIT models are completed by the explicit consideration, in the lattice instability mechanism, of the electron–phonon coupling [4]. They include Peierls-like or Fermi surface nesting scenarios which are well documented these days by the study of low dimensional metallic systems [5]. In the latter class, dominant electron–electron repulsions induce charge localization and, with the opening of a Mott–Hubbard gap, a spin–charge decoupling accompanied by antiferromagnetic correlations

between localized spins. Note however that these two kinds of mechanism are not mutually exclusive, so that both crystal structure and correlation effects should add their contribution in narrow band materials [6].

These days MIT are observed in a broad range of inorganic and organic materials [7]. Among them transition metal oxides (TMO) have been widely studied since the 1950's without, in most cases, obtaining a real consensus on the mechanism of the MIT. Difficulties of interpretation are due to the complexity of their electronic structure involving several sets of d orbitals [8]. TMO, which are narrow band materials and which thus exhibit sizeable electron–electron correlations, are also subject to structural instabilities (for examples many oxides are good ferroelectrics). All the difficulties to differentiate between the relative role of charge, spin and orbital electronic degrees of freedom and of their interaction with the atomic lattice degrees of freedom, generally subject to structural instabilities, are cumulated by the MIT of the vanadium dioxide VO_2.

For these reasons, special attention has been devoted to VO_2 for more than 50 years. VO_2 exhibits a clear example of a first order MIT at $T_{MI} = 340$ K from a d^1 rutile (R) tetragonal metallic phase to an insulating monoclinic (M_1) phase made of well decoupled V–V dimers. Indication of a phase transition was obtained in the 1930–1950's by the observation of a magnetic susceptibility drop [9, 10] together with a thermodynamic anomaly [11] at T_{MI}. The detection of a clear MIT was proved later by the observation of an abrupt conductivity drop at T_{MI} [12]. Note that the first report of an anomaly at T_{MI} in the thermal dependence of the conductivity is due to [13]. Soon after, [14] established, by recording the evolution of the diffraction spectrum of VO_2 through T_{MI}, that the MIT corresponds to a change of structure from a R phase towards a low symmetry monoclinic phase previously described in the literature [15,16]. The structural change, consisting of a unit cell doubling, was subsequently interpreted [14] as driving a non-magnetic ground state where d^1 electrons are paired in V–V spin singlets. However, the establishment by magnetic measurements of such a non-magnetic ground state in VO_2 took some time [17], because at that time an antiferromagnetic ground state was generally found in most of V oxides [18]. Note that the search for anti-ferromagnetism was the main motivation for the study of VO_2 in earlier times [9, 10, 13], and even in the first study of [18] VO_2 is incorrectly reported as an antiferromagnet below T_{MI}.

Important progress occurred in the 1970s, when taking into account the influence of the M_1 distortion on the t_{2g} electronic levels of the R metallic phase, [19] proposed a mechanism for the MIT of VO_2. Basically, this mechanism (more explicitly described in Section 5.1) combines an inter-band charge transfer process which leads to a half-filled quasi-1D $d_{//}$ band, within which a Peierls instability produces an insulating ground state through a lattice dimerization. In this mechanism occupied levels in insulating M_1 are the bonding states of the V–V dimers considered by [14].

New advances in the experimental study of the MIT of VO_2 occurred during the 1970's with the synthesis of alloys of VO_2, and the determination of their phase diagram. These earlier studies (reviewed by [20,21]) showed in particular that for substituents such as:

- Nb, which reduces the V, the substituted V–V pairs are killed, with the result of destabilizing the M_1 phase,
- Cr, which oxidizes the V, a new intermediate insulating M_2 phase is stabilized between R and M_1 in which half of the V sites form zig-zag chains where there is a Mott–Hubbard localization of d^1 electrons whose spins 1/2 are coupled antiferromagnetically.

While the former result supports the scenario of energy gain due to formation of well separated V–V pairs in M_1, the latter result shows that the electronic state of such pairs should be described in the Heitler–London limit. In other words, electron–electron correlations play a crucial role in the physical properties of insulating VO_2, a feature which is not considered in Goodenough's

mechanism of the MIT.

During the same years, a sizeable enhancement of the spin susceptibility [22] and of the electronic contribution at the heat capacity [23] was measured in metallic VO_2. Both features imply the presence of sizeable electron–electron interactions in the R phase. However, the mechanism responsible of such an enhancement (spin fluctuations in a strongly correlated gas, Stoner exchange enhancement or spin polaron effect considered in [20, 23, 24]) was unclear at that time. The main reason was the lack, in the 1970's, of *ab-initio* (for instance Local Density Approximation (LDA)) calculations of the true electronic structure and of an adequate formalism (for instance Dynamical Mean Field Theory (DMFT)) allowing, in presence of sizeable electron–electron repulsions, to consistently obtain the formation of Hubbard bands.

These first investigations raised a controversy between the so-called Peierls and Mott–Hubbard scenarios for the MIT of VO_2, which is not completely closed these days (see for example [25, 26]). In the 1970s, the controversy concerned also the relative contributions of the structural distortion and of electron–electron repulsions at the sizeable gap of charge ∼0.7 eV open in the M_1 phase (i.e., controversy between Peierls gap versus Mott–Hubbard gap). In addition, as the MIT is of 1st order, the controversy concerned also the dominant, lattice/phonon versus electron, contribution at the large entropy gain, of $1.5k_B$ per VO_2, which stabilizes the M_1 ground state.

In the last 20 years there has been a renewed interest in the study of the MIT of VO_2. This interest was motivated by the development of realistic electronic structure calculations, of new spectroscopic methods, using in particular synchrotron radiation, of ultrafast experimental investigation methods of the MIT and of dedicated means for elaboration of nanostructures such as thin films and nanowires [27, 28]. Also, the large change of conductivity and of dielectric properties at the MIT of VO_2, together with its reversible nature, and the large variation of T_{MI} under an external stimulus have triggered the development of many kinds of devices with a large number of potential technological applications. Potential applications of VO_2, which are presently the object of an intense international activity, concern, to name a few, smart windows, bolometer, actuators, transistor, hydrogen storage, thermochromic, nano-photonics. They are covered in recent reviews [27–30].

While there is an abundant literature on the electronic properties of VO_2, the lattice instability counterpart involved in the MIT is less well documented. In particular the pre-transitional lattice critical fluctuations observed long time ago in the metallic R phase [31] have not been deeply analyzed. The information thus deduced is an original contribution (Section 6) to the present review. In Section 2 we review the various crystal structures of VO_2 and in Section 3 its different phase diagrams upon alloying and external constraints. Analysis based on lattice symmetry considerations will be presented in Section 4. The salient electronic properties of the various phases of VO_2 will be commented in Section 5. In this section a complete analysis of the 1D localized magnetism in the insulating phases will be also presented. Structural fluctuations of the metallic rutile phase, pre-transitional at the MIT, will be analyzed in Section 6. Then structural contributions at the metal–insulator transition of VO_2 will then be discussed in Section 7, and, finally, some final remarks will be included in Section 8.

2. Crystal structures

These days it has been reported that, in addition to the 4 phases described in this section, VO_2 exhibits an important polymorphism. Five new phases of VO_2 as well as diagrams of phase transformation between them have been recently reviewed by [28]. Here in this section, we consider only the R, M_1, M_2 and T phases connected by the MIT of VO_2. Note also that poorly

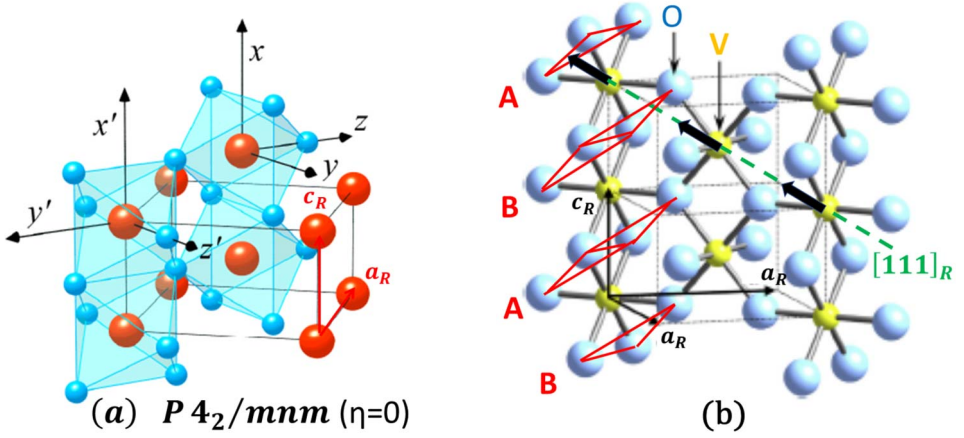

Figure 1. (a) Rutile structure of metallic VO_2 outlining in blue two chains of sharing edge VO_6 octahedra, related by 4_2 screw axis symmetry along c_R, of the unit cell. The (x, y, z) frame which corresponds to the principal directions of the electric field gradient (EFG) tensor on V site is indicated (Adapted from [33]. Copyright Wiley-VCH GmbH. Reproduced with permission). (b) Orientation of the rutile structure with respect to the ABAB hexagonal compact packing of oxygen layers outlined in red. Vanadium (in yellow) occupies one octahedral site out of two between two successive oxygen hexagonal layers. The $[111]_R$ direction of V displacement involved in the short range pre-transitional fluctuations at the MIT of VO_2 is also indicated.

documented additional phases appear for large doping (see Section 3.1) and under pressure (see Section 3.2.3).

2.1. *The rutile structure of metallic* VO_2

The rutile ($P4_2/mnm$) structure is very frequent among the inorganic compounds (for a recent review see [32]). This structure, whose prototype is exhibited by the band insulator TiO_2, is shown in Figure 1. It is derived from an ABAB type of compact packing of oxygen hexagonal layers, as shown in Figure 1b. In rutile structure the V occupy, between successive oxygen layers, one octahedral site out of two. As a consequence, each V is surrounded by an O octahedron. The V network forms a body centered tetragonal lattice, of parameters a_R and c_R, with two octahedra per unit cell related by 4_2 screw symmetry (Figure 1a). The V–V distance of 2.85 Å along the $[001]_R$ or c_R direction, is 20% smaller than the V–V second neighbors distance of 3.53 Å in the diagonal $\{111\}_R$ directions. Octahedra share two covalently O–O bonded edges in c_R direction, and two corner oxygens in $\{110\}_R$ directions.

The c_R/a_R ratio is considered by the literature [32] as an important quantity determining the general stability of the rutile structure MO_2. In metallic VO_2, the c_R/a_R ratio decreases in temperature, from 0.629 (at 573 K) to 0.626 (at 360 K) [34], reaching nearly the critical parameter ~0.625 below which the rutile structure should be unstable with respect to a low symmetry (generally monoclinic) distortion in which dimers, favoring direct M–M bonding, are formed [32]. This rule is however not followed for dopant reducing the V (see Section 3.1.1) because whatever the variation of the c_R/a_R ratio upon doping the M_1 phase is destabilized by the breaking of V–V pairs by the substituent. This is also the case of strained VO_2 films where the M_1 phase is destabilized by a deformation of oxygen octahedron accompanied by a decrease of the c_R/a_R ratio under constraint (see Figure 10).

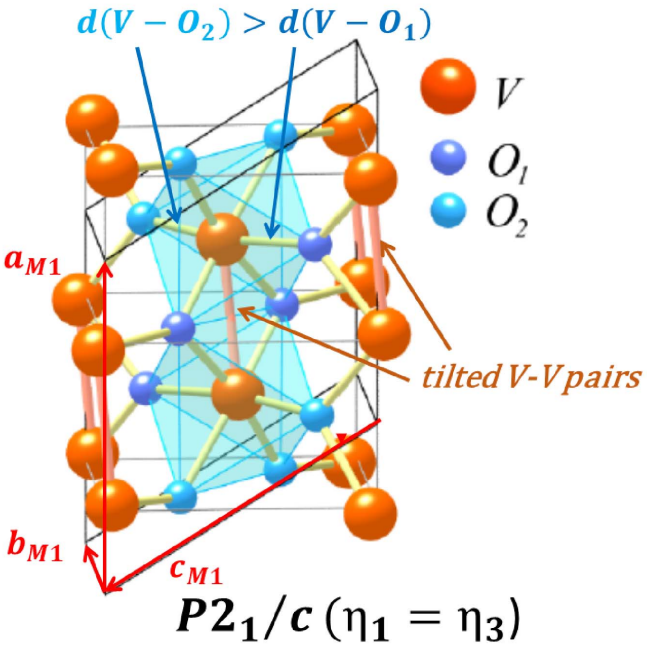

Figure 2. M_1 monoclinic structure of insulating VO_2 showing the two tilted V–V pairs, related by 2_1 screw axis symmetry along b_{M_1}, of the unit cell. The off-center V shift delimits short and long distances with O_1 and O_2 of the octahedron respectively. Two VO_6 deformed octahedra surrounding a V–V pair along a_{M_1}, and linked successively by short O_2–O_2 and long O_1–O_1 edges are represented in blue. In this structure all the V sites are equivalent. (Adapted from [33]. Copyright Wiley-VCH GmbH. Reproduced with permission)

2.2. V *displacement in the monoclinic* M_1 *and* M_2 *phases*

The 340 K MIT of VO_2 at ambient pressure stabilizes a V–V paired monoclinic M_1 phase of $P2_1/c$ symmetry corresponding to the MoO_2 structure [15, 16]—see Figure 2. The R to M_1 structural distortion can be better analyzed using the intermediate monoclinic M_2 structure [35] stabilized in stressed VO_2 and certain alloys (see Section 2.3).

The M_2 structure (Figure 3) breaks the symmetry relating the two equivalent octahedral V chain of the rutile structure by stabilizing two different types of V shifts: namely the formation of zig-zag V_2 chains running along c_R (a_{M_2}) and of a periodic array of V_1–V_1 pairs directed along c_R (a_{M_2}) (to avoid unnecessary complications we keep below the unit cell rutile notation). To this structure corresponds one of the two V distortion patterns schematically represented in Figure 4 that we shall name η_1 below. Of course, an equivalent distortion pattern where the two V sites of the rutile structure are interchanged is energetically equivalent (it is named η_3 in Figure 4). While the V in the M_2 ($C2/m$) structure adopts only one type η_i ($i = 1$ or 3) of distortion pattern, the V in the M_1 ($P2_1/c$) structure superimposes the η_1 and η_3 distortion patterns which are equivalent by symmetry. The M_1 structure is thus composed of equivalent chains made of paired zig-zag or tilted V–V pairs. The decomposition of V displacement into these two components plays a crucial role in the mechanism of the MIT of VO_2 proposed by [19]. Note that at that time Goodenough reasoned directly on the M_1 distortion, because the M_2 structure was not known.

M_1 and M_2 structures correspond to a sizeable deformation of the R structure. In M_2 the V zig-zag chains have a repeat distance of 2.93 Å and the V–V pairs, 2.54 Å long, are separated by

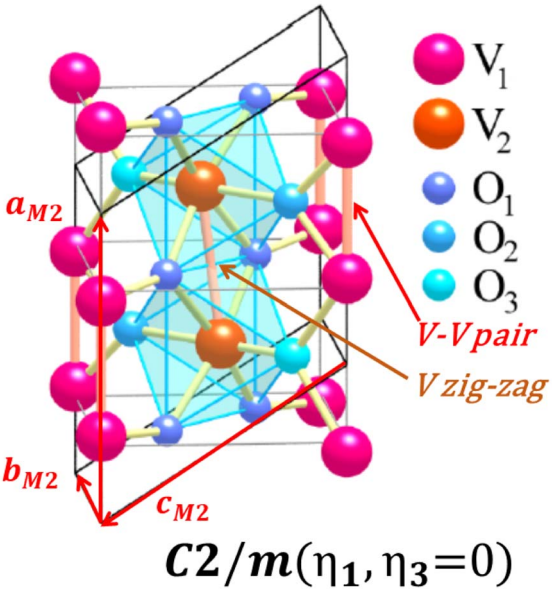

Figure 3. M_2 monoclinic structure of insulating VO_2 showing the alternation of V_2 zig-zag chains and of V_1–V_1 pairs directed along a_{M_2}. The two different V_1 and V_2 shifts induce three different types of oxygen atoms (O_1, O_2 and O_3) per unit cell. A chain of deformed VO_6 octahedra surrounding a V zig-zag running along a_{M_2} is shown in blue. (Adapted from [33]. Copyright Wiley-VCH GmbH. Reproduced with permission)

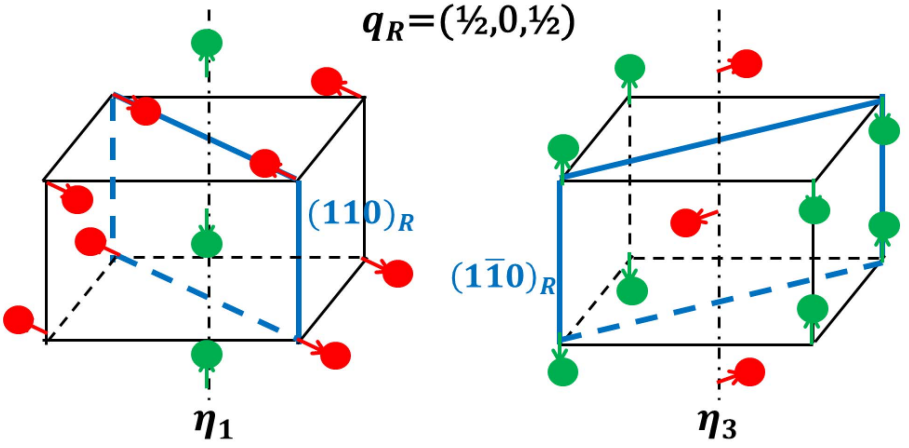

Figure 4. Degenerate η_1 and η_3 irreducible representations (IR) of the $\mathbf{q}_R$ small group of the rutile structure. Transverse and longitudinal V shifts with respect to c_R are indicated in red and green respectively (oxygen atoms are omitted). The red V form zig-zag chains along c_R while the green V form V–V pairs. Note that V shifts in η_1- and η_3-IR are respectively located in the orthogonal $(110)_R$ and $(1\bar{1}0)_R$ planes of the rutile structure outlined in blue.

3.26 Å [35]. These entities are formed by a V shift of ~0.2 Å from the center of the octahedron. V shifts of 0.23 Å (decomposed into a shift of 0.14 Å along c_R and a shift of 0.18 Å along the O apical direction) are found in the M_1 structure. They induce tilted V–V pairs which are 2.62 Å long

and separated by 3.18 Å [36]. By 2_1 screw axis symmetry, the pairing deformation is out of phase between neighboring chains (Figure 2). As a consequence of the V shift, VO octahedral distances vary sizably between 1.76 Å and 2.06 Å in M_1 structure [36]. A similar distribution of VO distances is found in the M_2 structure [35].

2.3. *The triclinic intermediate phase between* M_1 *and* M_2 *and probe of the* V *environment by electric field gradient measurements*

2.3.1. *The T phase*

The (η_1, $\eta_3 = 0$) M_2 structure transforms continuously into the (η_1, $\eta_3 = \eta_1$) M_1 structure by plugging a progressive η_3 distortion. This occurs by setting conjointly a dimerization of the V_2 zig-zag chain and a tilting of the V_1–V_1 pairs initially directed along c_R in the M_2 structure. This breaks the $2/m$ point symmetry of M_2, to $\overline{1}$ and thus a $P\overline{1}$ triclinic (T) structure results. The T structure can be well characterized on powder diffraction spectrum by the observation of significant angular splitting of some pseudo-rutile Bragg reflections [37–41]. The atomic positions in the T phase have been refined in $V_{1-x}Al_xO_2$ with $x = 1.5\%$ [42]. Two types of V–V pairs are formed: V_1–V_1 pairs whose internal distance decrease from M_1 to the M_2 phases, together with the vanishing of the tilt angles, and V_2–V_2 pairs whose internal distance increases from the M_1 to the M_2 phase, where zig-zag chains are formed. The correlation between the evolution of the two types of V–V distances between the M_1, T and M_2 phases is shown in Figure 5a (blue curve).

The M_2–T–M_1 transformation corresponds to a huge change of local symmetry around the V. These changes can be easily probed by local measurements such as ^{51}V NMR, and more particularly by the measurement of the electric field gradient (EFG) tensor on the V site [38].

2.3.2. *Electric field gradient probe of the* V *environment*

The symmetric EFG tensor can be expressed in a diagonal form (V_{xx}, V_{yy}, V_{zz} following the Poisson relationship: $V_{xx}+V_{yy}+V_{zz} = 0$) in an orthogonal frame of principal directions. From the point symmetry of the V site, these directions are the x, y and z symmetry axis of the O octahedron in the R structure (see Figure 1a). Note that these axes are rotated by 90° around the x axis between the two neighboring octahedra of the R unit cell. Of course, the principal axis deviates slightly from these directions in monoclinic structures when V shifts from the octahedron center and when O octahedra deforms. The experimental V EFG components measured by ^{51}V NMR are given in Table 1 for the R, M_1 and M_2 (V_1–V_1 pair entity) structures. The EFG cannot be measured on zig-zag V_2 (magnetic) sites in M_2. From experimental data there is an ambiguity of indexation of V_{yy}, V_{zz} due to the fact that y and z directions alternate between neighboring octahedra. This ambiguity has been recently resolved by EFG calculations [44]. This work shows in particular that the maxima value of the absolute EFG is along the apical z octahedral direction. Due to the Poisson relationship the diagonal EFG tensor, of zero trace, can be expressed by two quantities:

- the EFG absolute value ν_Q (here $|V_{zz}|$)
- the asymmetry parameter $\eta_Q = |(V_{yy} - V_{xx})/V_{zz}|$

also indicated in Table 1. According to the calculation of [44] V_{zz} is negative both in the R and M_1 phases.

Table 1 shows that there is large variation of the maximum EFG, ν_Q, and of the asymmetry parameter, η_Q, of the EFG in the different phases of VO_2. This confirms that the environment of V atoms changes considerably. It is noticeable that the EFG of the V_1 pairs in the M_2 phase is roughly the average between the EFG's in the R (at the MIT) and M_1 phases. The EFG in the rutile metallic phase of VO_2 varies sizably in temperature [45] at the difference of the EFG in the M_1 and

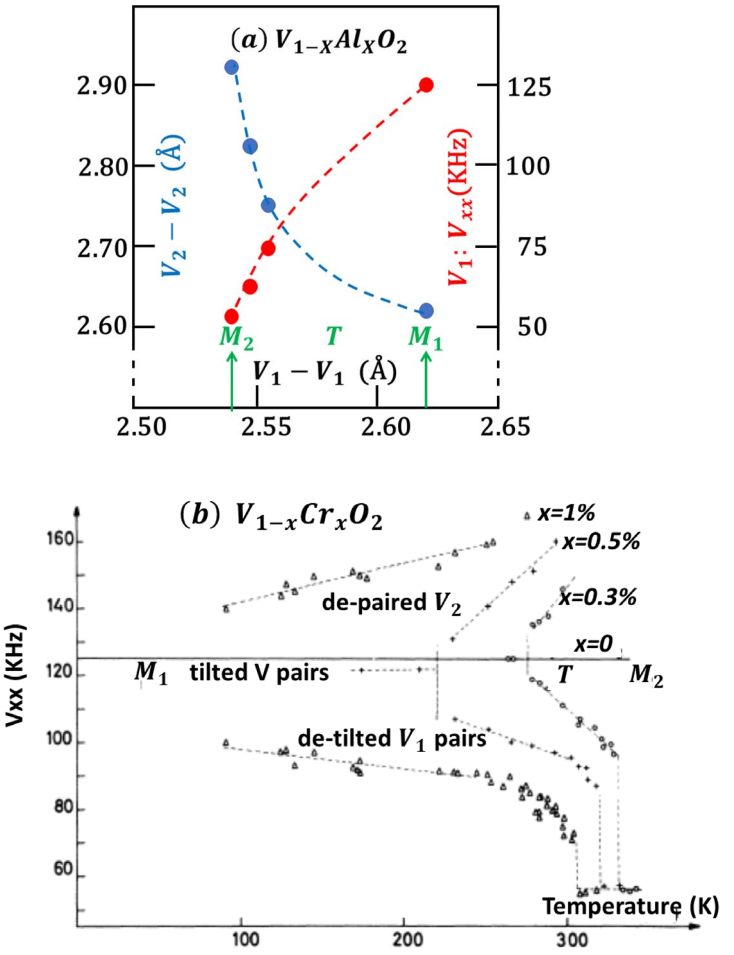

Figure 5. (a) Relation between V_2–V_2 and V_1–V_1 pair distances in the M_2, T and M_1 phase of $V_{1-x}Al_xO_2$ (blue curve) and correlation between the $^{51}V_1$ EFG component V_{xx} in function of the V_1–V_1 distance (red curve). These data combine the structural refinement of [42] for x = 1.5% with EFG measurements of [43] for x = 1.2%. (b) ^{51}V EFG component V_{xx} allowing to differentiate the two different V_1 and V_2 environments in the M_2 and T phases of $V_{1-x}Cr_xO_2$. These two EFG components merge into a single value when all the V sites become equivalent in M_1. Note the progressive differentiation of the two kinds of V site when the T phase evolves towards the M_2 phase (adapted from [38]).

M_2 insulating phases. This effect shall be related, in Section 5.2, to a variation in the occupation of *d* orbitals in metallic VO_2 on approaching T_{MI}.

Figure 5b gives the thermal dependence of two V_{xx} components associated with V_1–V_1 and V_2–V_2 pairs in the M_1, T and M_2 phases of the $V_{1-x}Cr_xO_2$. Starting from M_1 where all the V–V pairs are equivalent, one EFG component decreases when the V_1–V_1 pair distance decreases towards the one of M_2 phase, while the other EFG component increases when V_2–V_2 pair distance increases towards the V zig-zag distance in M_2 (because of the broadening of NMR spectra due to magnetism, V_{xx} cannot be measured in M_2 for the V zig-zag). These large and continuous EFG variations prove that the V environment changes sizably and progressively in the T phase between the one in the M_2 and M_1 phases. Similar results were obtained in $V_{1-x}Al_xO_2$ with

Table 1. Various determinations of the frequency (expressed in KHz) of the EFG tensor components on the V site in the R, M_1 and M_2 (V pair) along the x, y and z directions in the rutile phase indicated in Figure 1a (or close to these directions in the monoclinic phases)

Phase	$\lvert V_{xx}\rvert$ kHz	$\lvert V_{yy}\rvert$ kHz	$\lvert V_{zz}\rvert = \nu_Q$ kHz	η_Q	Reference
R (340 K) Pure VO_2	14	183	197	0.84	[45]
R (340–350 K) Pure VO_2	16(5)	187(6)	203(7)	0.84(2)	[44]
R (373 K) Pure VO_2	23	173	196	0.77	[46]
R (585 K) Pure VO_2	61	134	194	0.37	[45]
M_1 Pure VO_2	—	—	490(20)	0.50(2)	[47]
M_1 Pure VO_2	125(1)	368(2)	490(3)	0.49(1)	[38]
M_1 Ti dopant	121(3)	365(4)	486(5)	0.50(2)	[48]
M_1 Pure VO_2	115	373	488	0.53	[44]
M_2 (V_1 pair) Ti dopant	—	—	360(20)	0.65(2)	[49]
M_2 (V_1 pair) Cr dopant	56(1)	293(2)	349(3)	0.68(1)	[38]
M_2 (V_1 pair) Ti dopant	57(2)	294(3)	351(4)	0.68(2)	[48]
M_2 (V_1 pair) Al dopant	53	281	335	0.68	[43]

The thermal dependence of the EFG components in the R phase is more explicitly shown in Figure 13.

$x = 1.2\%$ [43]. Figure 5a reports for this last compound the correspondence between the lowest $^{51}V_1$ EFG component V_{xx} and the V_1–V_1 pair distance.

3. Phase diagrams

Just after the establishment in 1961 that the MIT of VO_2 is accompanied by a R to M_1 structural transition at 340 K [14], it was found that the R to M_1 T_{MI} critical temperature decreases sizably when V is substituted with Nb, Ta, Ti and Mo elements [50–52]. In the same time, some indications were found that an intermediate phase (now recognized as M_2) develops between the R and M_1 phases without a consequent destabilization of the M_1 phase in VO_2 containing traces of Ti [49], Al, Fe and Cr [53] impurities. This confusing situation required a detailed investigation of the phase diagram and of the structure of controlled solid solutions of VO_2, which started at the end of the 1960s [50–52, 54]. Following these works, we summarize, in part 1, the various phase diagrams of doped VO_2. Then, in part 2, we consider modification of the phase diagram of pure VO_2 under constraint (stress, strain and pressure).

3.1. VO_2 *and its alloys*

Figure 6 presents a schematic phase diagram of VO_2 and its alloys. Among them one must distinguish between:

(a) substituents such as Nb^{5+}, Mo^{6+}, W^{6+} and $Re^{5+/6+}$ donors which reduce V^{4+} into V^{3+}, or transfer one electron to the V network,
(b) substituents such as Cr^{3+}, Al^{3+}, Fe^{3+} and Ga^{3+} acceptors which oxidize V^{4+} into V^{5+} or transfer one hole to the V network,
(c) the Ti^{4+} substituent which does not transfer any charge to the V network,
(d) F substituent to O or non-stoichiometric VO_2 which modifies the cation–anion charge ratio.

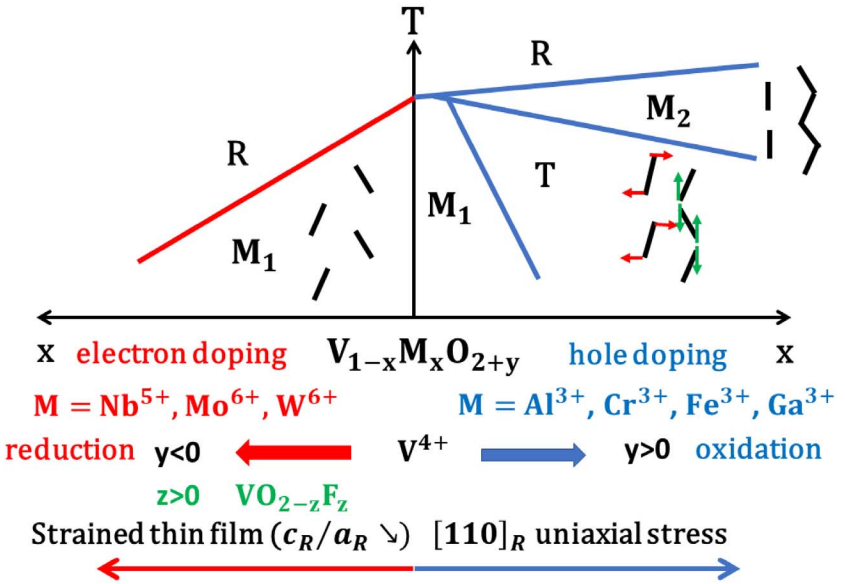

Figure 6. General phase diagram of doped, strained and stressed VO_2. V–V dimers and V zig-zag chains together with their evolution in the M_2, T and M_1 phases are schematically drawn. In the T phase the red and green arrows indicate the direction of V shifts following the progressive development of the η_3 order parameter defined in Figure 4.

All these substitutions modify sizably the phase diagram of pure VO_2, as schematically indicated in Figure 6. The physical studies of solid solutions, starting in the 1970's for bulk crystals, are all the more important these days because doped VO_2 thin films are currently used to realize devices having potential applications [27–30].

3.1.1. V *hole doping*

The R–M_1 MIT transition of VO_2 is kept with a small amount x of donor substituent such as Nb [55], W [56–58], Mo [59,60] and Re [61]. In the solid solution, with the insertion of bulky Nb^{5+}, Mo^{6+} and W^{6+} dopants, whose ionic radius (0.64, 0.59 and 0.60 Å respectively) is larger than the one of V^{4+} (0.58 Å), the parameters a_R and c_R of the R phase increase. However, the c_R/a_R ratio increases with Nb and W dopant while it decreases with Mo and Re dopant. But in all the solid solutions the insulating M_1 phase is strongly destabilized with increasing x. This general feature can be understood by the loss of M_1 stabilizing energy due to V–V pairing when in a given dimer the V is replaced by a substituent. For example, by substituting Nb to V, V^{4+}–V^{4+} pairs, where V^{4+} spins 1/2 are paired in a non-magnetic singlet, are broken into a $V^{3+}Nb^{5+}$ entities where the V^{3+} bears a spin 1 [22,62]. For x small, the MIT decreases by about 12(1) K per percent of V^{3+} formed.

However, for large x, different behaviors are found. Figure 7a presents the phase diagram of the $V_{1-x}Nb_xO_2$ solid solution [20,55,63]. The MIT saturates at ~250 K for x larger than 9% and becomes ill defined above this concentration. For x = 10% the insulating phase exhibits a long-range rutile (R′) order which is in fact an average structure. The true structure is made of locally disordered V–V tilted pairs. More precisely, the R′ phase presents a quite subtle local order which consists of a superimposition of two M_2 types of 2D orders respectively located in the $(110)_R$ and $(1\bar{1}0)_R$ planes shown in Figure 4. This corresponds also to a disorder in the tilt angle of the V–V pairs in a third direction perpendicular at each type of the above quoted plane [31]. More concisely, each 2D M_2 order is recovered by spatial averaging to zero of one of the two η

components of the (η, η) M_1 order parameter. Note that if the spatial average is only performed on a single η component of the M_1 order parameter, a monoclinic M′ average long-range order is obtained. It is observed between $7\% < x < 9\%$ (see Figure 7a). These short-range orders, which extend on ~100 Å, vanish upon heating towards the transition towards the metallic R phase.

A completely different phase diagram, shown Figure 7b, is obtained for large x in the $V_{1-x}Mo_xO_2$ solid solution [60]. T_{MI} decreases linearly when x increases, in such a way that a low temperature correlated metallic state is stabilized for $x > 0.2$. However, in this concentration range superconductivity is not detected down to 0.35 K. The stabilization of a low temperature metallic state is also reported for large x in $V_{1-x}W_xO_2$ [23, 58].

3.1.2. V *electron doping*

The phase diagram of VO_2 substituted with Cr^{3+}, Fe^{3+}, Al^{3+} and Ga^{3+} acceptors, whose ionic radius (0.62, 0.55, 0.53 and 0.62 Å respectively) is comparable to the one of V^{4+} (0.58 Å), is very different from the phase diagram obtained with donors. Very early a new insulating phase whose symmetry and magnetic properties are different from those of M_1 was detected in $V_{1-x}Fe_xO_2$ [17] and $V_{1-x}Cr_xO_2$ [64] solid solutions. Also, at the difference of hole doped systems considered previously, the MIT of electron doped systems was found to increase with x. However, the first published phase diagrams were incomplete with regard to the number and of the structure of new phases stabilized between the R and M_1 phases of pure VO_2. It is now well established that two new insulating M_2 and T phases were found to intercalate for small amount of Cr [37, 38], Al [39, 43, 65], Fe [40, 66, 67] and Ga [41, 68, 69]. Note that the triclinic T phase is sometimes still incorrectly named in the literature as the monoclinic M_3 phase, a variant of M_2, previously suggested in $V_{1-x}Cr_xO_2$ [35]. These intermediate phases, described in Section 2, differentiate the two components of V shift in the M_1 phase. The phase diagrams of these solid solutions show common characteristics with that of $V_{1-x}Cr_xO_2$ shown in Figure 8. The R–M_2 transition is of first order. From EFG (Figure 5) and structural measurements (i.e., from the angular splitting of pseudo-rutile Bragg reflections) the M_2–T transition is also first order, while the T–M_1 transition is basically continuous. The critical temperature of the T–M_1 phase transition abruptly decreases with increasing x, so that the M_1 phase vanishes above $x \sim 1\%$.

At ambient pressure, between $x = 8\%$ and 15% of Cr in the $V_{1-x}Cr_xO_2$ solid solution a new monoclinic pseudo rutile M_4 ($P2/m$) insulating phase replaces the M_2 and T phases (Figure 8). In this phase V pairing apparently vanishes (on average?) [37]. The M_4 phase is also stabilized between $x = 5\%$ and 11% of Fe in the $V_{1-x}Fe_xO_2$ solid solution, while for x between 11% and 13% an orthorhombic O phase appears and for x between 13% and 25% another phase of unknown symmetry is reported [66].

3.1.3. *The special case of Ti substituent*

It was noticed in earlier studies of VO_2 that minute substitution of V^{4+} by Ti^{4+} intercalates a new insulating phase between the R and M_1 phases of pure VO_2 [48, 49, 70]. From EFG measurements this phase can be identified as M_2 [48, 49]. EFG measurements also show that upon cooling there is a 1st order M_2 to M_1 transformation [49] without the detection of the intermediate T phase present in the phase diagram of acceptor dopants. As for the electron doped systems, the R–M_2 transition temperature increases with x, the amount of Ti, and for $x > 13\%$ a new M_4 phase is stabilized [71].

3.1.4. *Anion substitution and oxygen non stoichiometry*

The M_1 phase of VO_2 is destabilized when a fraction z of divalent O is replaced by the monovalent F on the anionic sublattice. The solid solution $VO_{2-z}F_z$ thus incorporates a fraction z of V^{3+}. Also, the rate of decrease of T_{MI} per V^{3+} formed is the same as for V hole doping [72].

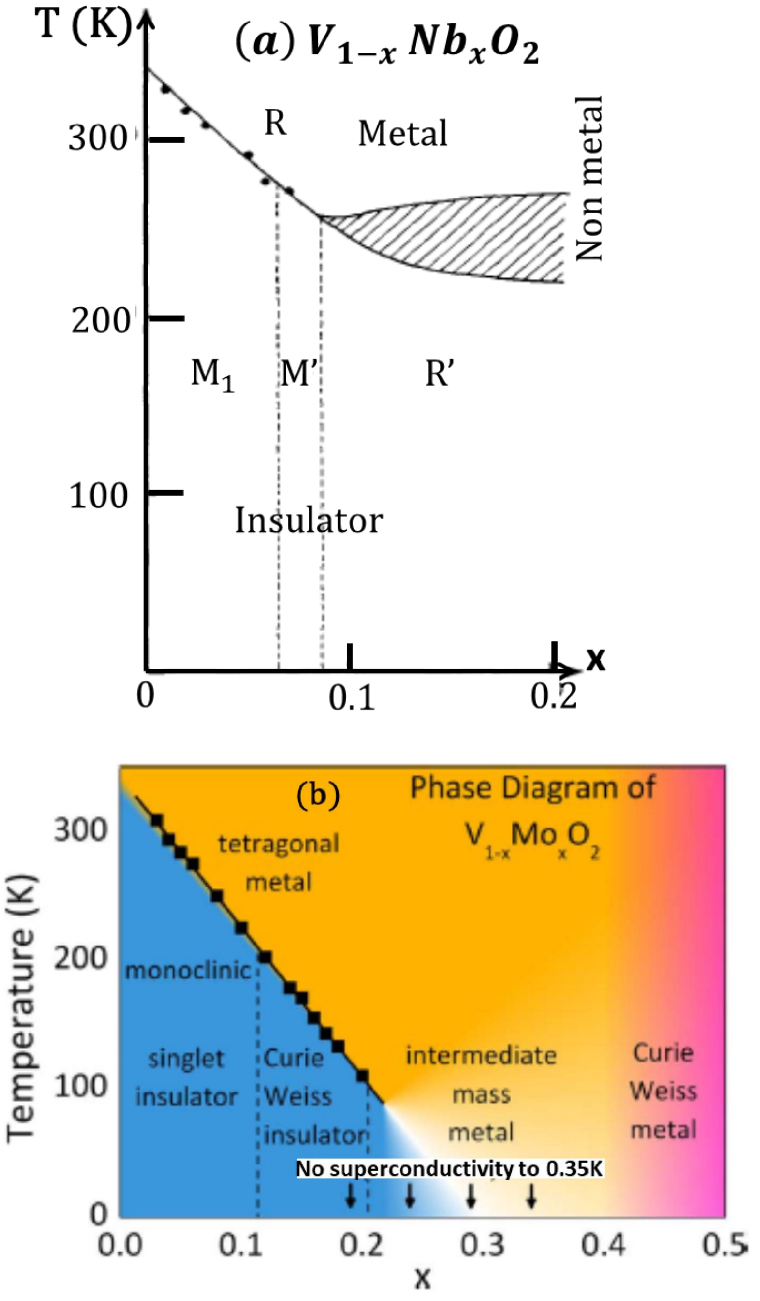

Figure 7. Phase diagrams of $V_{1-x}Nb_xO_2$ (a) and $V_{1-x}Mo_xO_2$ (b) according to [60, 63] respectively. Note that with increasing x, while the metallic R state is stabilized down to low temperature for $x > 0.2$ in Mo alloys, a non-metallic R state (due to a Mott–Hubbard charge localization) is observed for $x > 0.2$ in Nb alloys.

Although F^- has an ionic radius (1.33 Å) smaller than the one of the O^{2-} (1.40 Å), the a_R, c_R and c_R/a_R parameters sizably increase with z.

Oxygen non stoichiometry, y, has also a profound influence on the phase diagram of solid so-

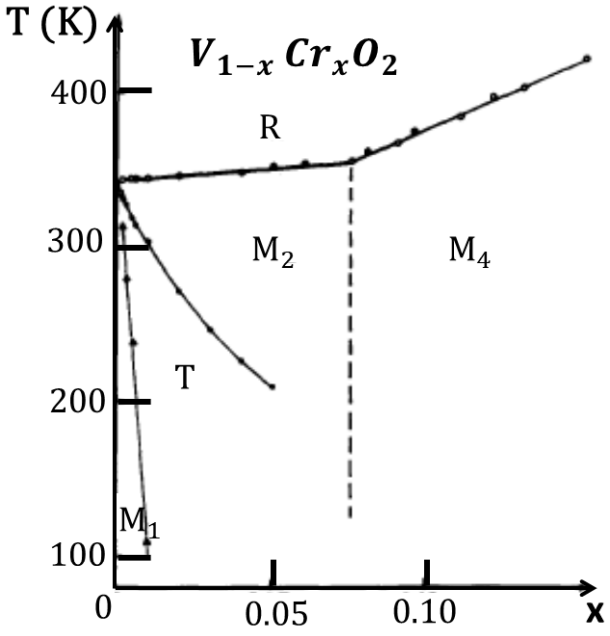

Figure 8. Phase diagram of $V_{1-x}Cr_xO_2$ according to [37].

lutions of VO_2, especially in presence of V substituents such as M = Cr, Al, Ga, Fe. In $V_{1-x}M_xO_{2+y}$ oxygen non stoichiometry changes the number of V^{3+} present in the solid solution to $x+y$. It is found in particular that oxygen deficiency ($y<0$) compensates the effect of M^{3+} doping [73]. This induces a vanishing of the M_2 and T phases, as observed in the Al doped systems [43]. In a similar manner, it is found in the solid solution $V_{1-x}Cr_xO_{2-x}F_x$ that when $x=z$ increases the M_1 phase spreads at the expense of the M_2 and T phases [74]. In an opposite manner, oxygen excess ($y>0$) in $V_{1-x}Al_xO_{2+y}$ increases the stability of the M_2 phase [43].

3.1.5. *Irradiation defects*

The MIT of VO_2 has been studied upon irradiation with O^+ ions [75]. Irradiation of VO_2 leads to a much milder reduction of the MIT and T_{MI} and to a weak gradual decrease of the insulating state resistivity compared to V_2O_3, showing that the insulating state and the MIT of VO_2 are much more robust and less susceptible to disorder than for V_2O_3. Structural measurements, on the other hand, are insensitive to irradiation with O^+ ions, thus indicating that no major structural changes or formation of secondary phases occur. This means that irradiation probably induces local perturbation breaking the M_1 V–V pairs of VO_2. In this respect, it has been proposed that such point defects consist in V and O local displacement forming vanadium and oxygen Frenkel pairs [76].

3.2. *Stressed, strained and pressurized* VO_2

3.2.1. *Stressed* VO_2

By applying an uniaxial stress along the $[110]_R$ direction (i.e. along the local z and y' octahedral directions shown in Figure 1a) in the R or M_1 unit cell of VO_2 the V sites and O octahedra become differentiated. A shear unit cell deformation towards the T phase is induced and the equivalent V of pure VO_2 in ambient condition now experience different environments, as proven by EFG

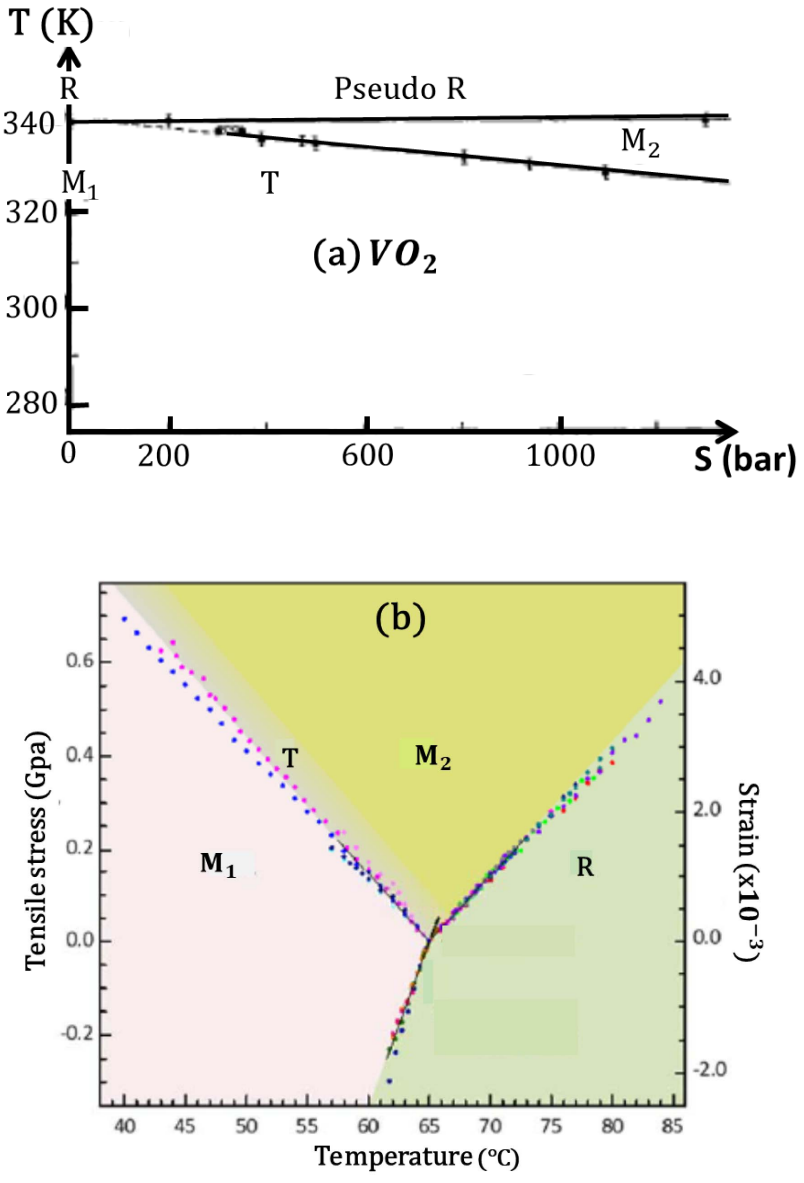

Figure 9. (a) Phase diagram of $[110]_R$ stressed VO_2 (from [77]). (b) Tensile stress–temperature phase diagram of VO_2 nanobeam (from [78]).

measurements. Modest stresses of few hundred of bar then induce the M_2 phase, just below the metallic R phase. The phase diagram thus deduced from NMR and ESR local measurements is shown in Figure 9a [77]. One recovers the phase diagram of acceptor doped systems, previously discussed in part 3.1b.

Recent experiments have determined the stress–temperature phase diagram by applying a uniaxial stress along c_R in free standing micro/nanocrystals of VO_2. As a function of the temperature a M_1, M_2 and R phase diagram is constructed. These different phases have been characterized by combining in situ microscopic imaging and micro-X-ray diffraction on single

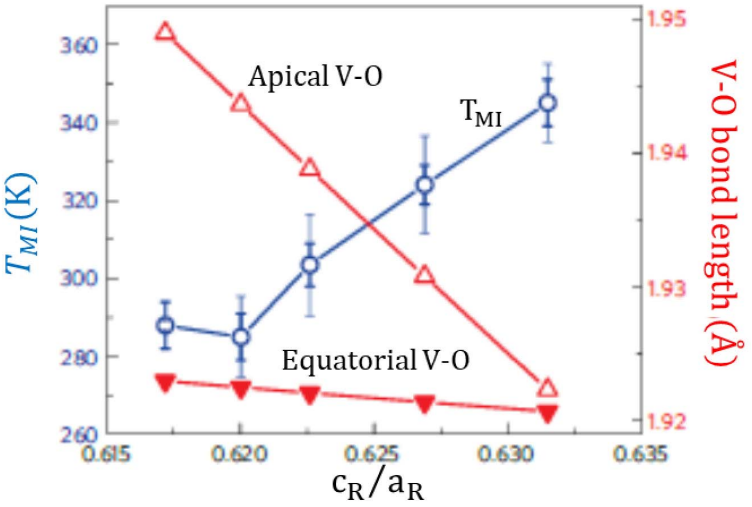

Figure 10. Variation of T_{MI} in stressed VO_2 films in function of the c_R/a_R ratio in the R phase. The variation of V–O bond lengths for both equatorial and apical oxygens in R phase is also shown (from [81]).

domain of crystalline VO_2 microbeams [79]. The tensile stress–temperature phase diagram of VO_2 has been also determined using single-crystal VO_2 nanobeams placed in a nanomechanical axial strain apparatus [78]. The phase diagram thus obtained (Figure 9b) reveals the presence of M_1, M_2 and R phases which surprisingly merge into a solid-state triple point found at 338 K ($\approx T_{MI}$) for unstrained VO_2. In the phase diagram of [78] the T phase between M_1 and M_2 is metastable. This finding is contradicted by a determination using micro-Raman spectroscopy of the (T, tensile strain) phase diagram which reveals a stable T phase around RT and under modest strain in single crystal VO_2 microbeams [80]. Furthermore, this last study shows that the M_1–T transition is continuous while the T–M_2 and M_1–M_2 transitions are first order, in agreement with results obtained in acceptor doped (Section 3.1.2) and Ti substituted (Section 3.1.3) VO_2 systems.

Finally, note that additional complication should occur in the determination of the tensile stress–temperature phase diagram of VO_2 micro- and nano-beams because M_1, M_2 and R domain patterns are observed [78, 79]. Also, as VO_2 is an (improper) ferro-elastic material, the formation of domains should affect local strain distribution and hence perturb the experimental conditions to establish the MIT phase diagram (for more detail see Section 4.2.3).

3.2.2. *Strained* VO_2 *films*

Strained VO_2 is obtained by epitaxial deposition of a VO_2 thin film on substrates such as TiO_2 (001) and (110). A large reduction of T_{MI} is observed by deposition on TiO_2 (001) substrate, while an enhancement of T_{MI} is obtained on TiO_2 (110) substrate [82]. Note however that with such a procedure, biaxial strain could result from lattice mismatch between VO_2 and the substrate. Thus, measurements have been redone in a more controlled manner with VO_2 thin films placed on a RuO_2 buffer layer deposited on TiO_2 (001) substrate [81]. This device allows, through the buffer thickness, a precise control of the a_R expansion (c_R contraction) of the VO_2 film. It is found (Figure 10) that T_{MI} decreases when the c_R/a_R ratio decreases. This is a surprising result because it is stated in the literature on empirical considerations [32] that M_1 pairing is stabilized when the c_R/a_R ratio decreases. However, it appears that in their experimental conditions strained VO_2 films undergo a sizeable octahedral deformation: strong increase of the

V–O apical distance without appreciable change of the equatorial V–O distance (see Figure 10). This deformation should significantly change the relative occupancy of the V t_{2g} orbitals in metallic VO_2. In particular X-ray absorption spectroscopy of such films provides evidence of a charge transfer from $d_{//}$ to π^* orbitals (defined in Section 5) under uniaxial strain [81].

3.2.3. *Pressurized* VO_2

These last years the improvement of experimental technics has opened the route to the study of pressurized materials. In spite of that the phase diagram of VO_2 under pressure remains largely incomplete. From Raman and electrical measurements, the metal–insulator transition T_{MI} increases up to 370 K for 18 GPa and decreases for higher pressures, reaching 300 K for ~38 GPa [83]. At ambient temperature pressurized M_1 VO_2 phase exhibits above 11 GPa (P*) a net enhancement of its optical conductivity [84] and a faster rate of increase of its electrical conductivity [85]. According to [85] the stable phase for $P > P^*$, denoted by the notation M_1^* in the literature, could be associated to a progressive band gap closure. However, X-ray diffractogram does not provide any evidence of change of $P2_1/c$ symmetry on crossing P^* [85–87]. Only a remarkable anisotropic compression in the $(b,c)_{M_1}$ plane is noticeable on crossing P^* [86]. However, since the M_1^* structure has not been refined, it is not known if a possible rearrangement of V chains accompanied by a variation of $3d$ t_{2g} V occupancy occurs. The enhanced conductivity saturates around 40 GPa. At these pressures another unknown metallic phase, characterized by a different powder diffraction pattern [85], should be stabilized. Recent Raman scattering and X-ray diffraction data evidence another structural modification around 19 GPa towards a different monoclinic M_3 phase [87].

4. Lattice symmetry considerations

4.1. *The four-component order parameter*

The monoclinic M_1 unit cell of VO_2 is obtained from the rutile R unit cell by the transformation [16]:

$$\begin{pmatrix} a_{M_1} \\ b_{M_1} \\ c_{M_1} \end{pmatrix} = \begin{bmatrix} 0 & 0 & 2 \\ 0 & 1 & 0 \\ 1 & 0 & -1 \end{bmatrix} \begin{pmatrix} a_R \\ a_R \\ c_R \end{pmatrix} \tag{1}$$

This transformation implies a doubling of the rutile unit cell to which corresponds the setting of new reciprocal periodicities at the reduced R point $\mathbf{q}_R = (1/2, 0, 1/2)_R$ at the boundary of the rutile Brillouin zone (designated by the subscript R). The M_1 unit cell doubling can also set new reciprocal periodicities at $\mathbf{q}_{R'} = (0, 1/2, 1/2)_R$, which is equivalent to $\mathbf{q}_R$ by rutile reciprocal space symmetry. The star of the R to M_1 structural transformation thus contains 2 arms ($\mathbf{q}_R$ or $\mathbf{q}_{R'}$) in reciprocal space. However only one arm of the star is activated in the R to M_1 (or M_2) phase transformation. The irreducible representation (IR) of the R → M_1 phase transformation has for each arm two degenerated components η_1 and η_3 [88], whose elementary V shifts in the rutile unit cell are represented in Figure 4. V shifts are interchanged between η_1 and η_3. To summarize, the order parameter of structural transitions of VO_2 has 4 dimensions: $\mathbf{q}_R$ and $\mathbf{q}_{R'}$ arms, each degenerated two times. Such order parameter can thus be expressed in the vectorial (η_1, η_2, η_3, η_4) form. In this notation the two degenerated η_1 and η_3 RI are associated to $\mathbf{q}_R$, and η_2 and η_4 RI are associated to $\mathbf{q}_{R'}$. If $\mathbf{q}_R$ is relevant, η_1 and η_3 are both activated in the R to M_1 transition, but only η_1 or η_3 is activated in the R to M_2 transition.

4.2. *Landau theory*

The description of the complex R–M_1–T–M_2 structural phase diagram of the $V_{1-x}Cr_xO_2$ solid solution (Figure 8) has motivated an elaborated Landau theory investigation of phase transitions in systems with a 4-components order parameter. This phenomenological theory was developed to establish the stable phase diagram of VO_2 and its alloys and VO_2 under external constraints. As there is an important literature concerning the symmetry analysis of the structural transitions of VO_2, especially by the Russian school in the 1970's, we shall quote below only the most important references.

4.2.1. *Free energy expansion up to the 6th order*

As the R–M_1 MIT of VO_2 is first order, the minimal expansion of the free energy must be of the 6th order in the η_i components of the order parameter. The expansion built on the different invariants of the four η_i RIs of the $\mathbf{q}_R$ and $\mathbf{q}_{R'}$ arms has been first derived by [88]. This functional can be expressed for a phase transition at T_c, using the notations of [89], as:

$$F = \frac{a}{2}(T - T_c)\sum_i \eta_i^2 + \frac{1}{4}\sum_{i,j} b_{ij}\eta_i^2\eta_j^2 + \frac{1}{6}\sum_{i,j} d_{ij}\eta_i^2\eta_j^4 \tag{2}$$

It describes four types of symmetry breaking transitions indicated by the 4 first lines in Table 2, where the symmetry of low temperature phases is specified by one or two finite and identical η values. The symmetry breaking involves two phases, M_1 and M_2, where only one arm of the star ($\mathbf{q}_R$ in the table) is activated and two phases for which the two $\mathbf{q}_R$ and $\mathbf{q}_{R'}$ arms of the star are conjointly activated. Note that up to the 6th order in the free energy expansion, the T phase is not stable.

By defining the vectorial order parameters of the M_1 and M_2 phases of VO_2 by:

$$\eta_{M_1} = \tfrac{1}{\sqrt{2}}(\eta, 0, \eta, 0) \quad \text{and} \quad \eta_{M_2} = (\eta, 0, 0, 0) \tag{3}$$

the free energy of the phase α (M_1 or M_2) reads:

$$F_\alpha = \frac{a}{2}(T - T_c)\eta^2 + \frac{1}{4}b_\alpha\eta^4 + \frac{1}{6}d_\alpha\eta^6 \tag{4}$$

Using the fact that by symmetry one has $b_{11} = b_{33}$ and $b_{13} = b_{31}$ in (2), one gets $b_{M_1} = (b_{11} + b_{13})$ and $b_{M_2} = b_{11}$ in (4). Note that because the R–M_1 and R–M_2 transitions are first order one has $b_\alpha < 0$. Similar expressions are obtained for d_α (α being M_1 or M_2) introduced in (4) in function of the d_{ij}'s defined in (2). The condition $d_\alpha > 0$ insures the stability of M_1 and M_2 phases. At T_c the minimization of (4) with respect to η leads to:

$$\eta^2 = -\frac{b_\alpha}{d_\alpha} \quad \text{and thus } F_\alpha = \frac{{b_\alpha}^3}{12{d_\alpha}^2} \tag{5}$$

By defining $\beta = b_{M_1}/b_{M_2}$ and $\delta = d_{M_1}/d_{M_2}$, the phase M_1 is more stable than M_2 if $\beta^3 > 12\delta^2$ and the phase M_2 is more stable than M_1 if $\beta^3 < 12\delta^2$ [89]. It is found from latent heat measurements in the $V_{1-x}Cr_xO_2$ solid solution that the phase M_1 is more stable than the phase M_2 [38]. This finding can be understood by the presence of an excess of entropy due to magnetic fluctuations in the zig-zag spin $(1/2)V^{4+}$ Heisenberg chains in the M_2 phase (see Section 5.3). Note that stress should renormalize the b_α coefficients (see part c below).

4.2.2. *General expansion of the free energy*

It was very soon realized that obtaining of the T phase of VO_2 required a general expansion of the free energy up to the 8th order in the order parameter [90]. This expansion allows for stabilization of 5 additional phases, one phase (i.e., T) with a single $\mathbf{q}_R$ modulation and 4 phases with a simultaneous $\mathbf{q}_R$ and $\mathbf{q}_{R'}$ modulation (Table 2). In these five new phases the order

Table 2. Low symmetry phases stabilized by a $\mathbf{q}_R/\mathbf{q}_{R'}$ instability of the rutile structure

Vectorial order parameter	Critical wave vector	Space group stabilized	Multiple of R volume
$(\eta,0,0,0)$	$\mathbf{q}_R$	$C2/m$ (M_2)	2
$(\eta,\eta,0,0)$	$\mathbf{q}_R$ and $\mathbf{q}_{R'}$	$Fmmm$	4
$(\eta,0,\eta,0)$	$\mathbf{q}_R$	$P2_1/c$ (M_1)	2
$(\eta,0,0,\eta)$	$\mathbf{q}_R$ and $\mathbf{q}_{R'}$	$I4_1/a$	4
$(\eta,\eta',0,0)$	$\mathbf{q}_R$ and $\mathbf{q}_{R'}$	$C2/m$	4
$(\eta,0,\eta',0)$	$\mathbf{q}_R$	$P\bar{1}$ (T)	2
$(\eta,0,0,\eta')$	$\mathbf{q}_R$ and $\mathbf{q}_{R'}$	$C2/c$	4
(η,η,η',η')	$\mathbf{q}_R$ and $\mathbf{q}_{R'}$	$P2_1/c$	4
$(\eta_1,\eta_2,\eta_3,\eta_4)$	$\mathbf{q}_R$ and $\mathbf{q}_{R'}$	$P\bar{1}$	4

The first 4 phases are obtained by minimization of the free energy expansion (2) up to the 6th order, while the additional last 5 phases are obtained for the free energy expansion up to the 8th order. Note that the 3 single $\mathbf{q}_R$ phases of this table are observed in VO_2 and its alloys.

parameter presents different η components as indicated in Table 2. The general list of stable phase diagrams, where the order parameter transforms as a four dimensions representation of 3D space groups, has been classified by [91]. Here we consider only the phase diagram for a single $\mathbf{q}_R$ modulation which is the case of VO_2.

In the phase transition of VO_2 where only one arm of the star with a degenerated (η_1, η_3) IR is activated, the free energy expansion is equivalent to the one obtained for a two-component order parameter ($\eta_1 = \rho\cos\phi, \eta_3 = \rho\sin\phi$) which transforms according to the C_{4v} point group [92]. This type of functional has been also used to analyze in detail the structural phase diagram of layered perovskite [93]. With this two-components order parameter two invariants can be constructed:

$$I_1 = \eta_1^2 + \eta_3^2 = \rho^2 \quad \text{and} \quad I_2 = (\eta_1^2 - \eta_3^2)^2 - 4\eta_1^2\eta_3^2 = \rho^4\cos 4\phi \tag{6}$$

From them one simply derives the free energy expansion up to the 8th order [92,93]:

$$F = a_1 I_1 + a_2 {I_1}^2 + a_3 {I_1}^3 + a_4 {I_1}^4 + b_1 I_2 + b_2 {I_2}^2 + c_{12} I_1 I_2 + c_{112} {I_1}^2 I_2 \tag{7}$$

Minimization of this free energy is obtained for 4 different sets of order parameters:

- $\eta_1 = \eta_3 = 0$ or $\rho = 0$, which corresponds to the R high temperature phase,
- $\eta_1 \neq 0$, $\eta_3 = 0$ or $\rho \neq 0$ and $\sin\phi = 0$, which corresponds to the M_2 phase,
- $\eta_1 = \eta_3 \neq 0$ or $\rho \neq 0$ and $\sin\phi = \cos\phi$, which corresponds to the M_1 phase,
- $\eta_1 \neq \eta_3 \neq 0$ or $\rho \neq 0$ and $\sin\phi \neq \cos\phi$, which corresponds to the T phase.

Figure 11 represents schematically the 3 generic phase diagrams obtained in function of the parameters of the free energy expansion (7). Lines of second order and of first order transitions are differentiated in this figure. There are only two types of triple points where the first order transition lines between R, M_1 and T or R, M_2 and T phases merge and one quadruple point where all the second order transition lines between the R, M_1, T and M_2 phases merge. These phase diagrams do not exhibit the R, M_1, M_2 triple point reported in Figure 9b. A first order R to T phase transition (left side of Figure 11) is not observed except perhaps for a weak $[110]_R$ stress applied to VO_2 (Figure 9a).

These phenomenological phase diagrams predict a first order R–M_1 phase transition when, for b_1 positive enough, a_1 decreases. However, the diagram intercalating the 1st order R–M_2 and M_2–T phase transitions requires a large increase of b_1 starting from negative values (for which M_2 is stabilized) in the phase diagram obtained with $a_1 < 0$ and $\Delta < 0$ (left side of Figure 11). According to the Landau theory, b_1 appears to be the critical parameter controlling the sequence

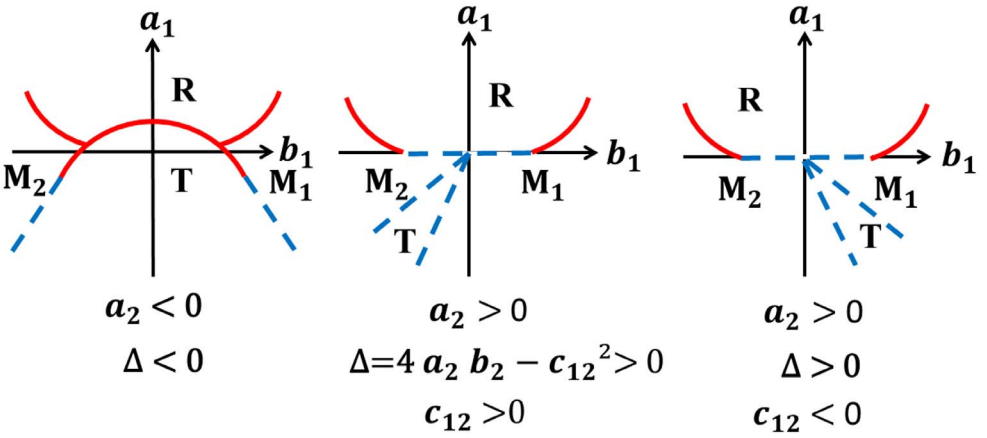

Figure 11. Schematic phase diagrams of the Landau free energy (7) in function of the coefficients of its expansion. The dashed (blue) and continuous (red) lines are second and first order transition lines respectively. The phases indicated are those of VO_2 (adapted from [92]).

of insulating phases of VO_2. This was already assessed in part (a) by the introduction of the ratio β. Here, with the inclusion of the phase ϕ in the definition of the order parameter, I_2 and consequently b_1 should change of sign between M_2 ($\phi = 0$) and M_1 ($\phi = \pi/4$). Note however that this type of analysis should not be pushed too far because when order parameter fluctuations are taken into account second order transition lines, obtained in the other phase diagrams of Figure 11, can be transformed into first order transition lines (see part 4.3).

4.2.3. *Ferro-elasticity and coupling to strain*

The R–M_1 and R–M_2 MITs of VO_2 are accompanied by a change of lattice symmetry from quadratic ($4/mmm$ point group) to monoclinic ($2/m$ point group). These transitions are thus ferro-elastic. The spontaneous elastic deformation of the unit cell which results can be also taken as an order parameter of the transition. The spontaneous deformation (strain) tensor of VO_2 is given by [94]. Since the MIT involves primarily a unit cell doubling, the spontaneous lattice deformation is a secondary order parameter of the transition, and for that reason the ferro-elastic transition of VO_2 is called improper. In that case it is expected when T_{MI} is approached from below a partial softening of the elastic constants related to the spontaneous deformation [94]. Indeed, it has been found from Rayleigh sound velocity measurements [95, 96] a softening of the stiffness coefficient C_{44} by ~20% and of $(C_{11}–C_{12})/2$ by ~40% in the M_1 phase.

A general symmetry analysis of the ferro-elastic coupling between primary and secondary order parameters has been performed by [97], see also [98]. The different types of coupling between the two components (η_1, η_3) primary order parameter of VO_2 and a secondary order parameters ζ are given by [93]. At the lowest order in development of the order parameters there are two types of coupling terms:

$$(\eta_1^2 \pm \eta_3^2)\zeta \tag{8a}$$

$$\eta_1\eta_3\zeta \tag{8b}$$

Only (8a) gives a coupling with the strain tensor e_{ij}. It is more explicitly expressed via the two coupling terms:

$$(\eta_1^2 - \eta_3^2)e_{xy} \tag{9}$$

$$(\eta_1^2 + \eta_3^2)[\lambda(e_{xx} + e_{yy}) + \mu e_{zz}] \tag{10}$$

However, in (10) the coupling to a uniaxial longitudinal strain e_{zz} (or any strain $\lambda(e_{xx} + e_{yy}) + \mu e_{zz}$), does not break the R tetragonal symmetry. It only renormalizes coefficients of the bare Landau development (2). Thus, only the coupling to the shear strain e_{xy}, given by (9), modifies the phase diagram of pure VO_2. This coupling lowers the free energy of the M_2 phase, for which $\eta_3 = 0$, but does not modify the free energy of the M_1 phase where $\eta_1 = \eta_3$. Thus, the shear stress e_{xy} suppresses the M_1 phase and stabilizes the M_2 phase, as experimentally observed in Figure 9a [77].

In VO_2 single crystal, 4 types of domains related by the point symmetry elements lost at the MIT are formed [94]. All these domains have been observed [99]. Furthermore, the domain structure is modified under stress. According to the analysis developed by [89] e_{xz} stabilizes one domain of phase M_1. The stress $(e_{xx}–e_{yy})$ keeps the degeneracy of M_1 and M_2 at T_{MI} but nonlinear b_{13} and d_{13} terms in the expansion (2) should stabilize the phase M_1, as in unstrained sample.

The experimental situation is more subtle in VO_2 nano-systems with the observation of M_1, M_2 and R domain patterns at the MIT, see for example stress experiments quoted in part 3.2a. However, it has been argued [89] that in unconstrained VO_2, M_1 should be the stable lower-symmetry phase in ambient condition. But a small perturbation, which renormalizes coefficients b_{ij} of the Landau free energy development (2), allows the stabilization of the M_2 phase with respect to M_1 or the coexistence of M_1, M_2, and R phases. The interplay between ferro-elasticity and MITs in strained VO_2 nanoplatelets has been experimentally demonstrated by [100]. Also, mesoscopic strain-induced MITs in the vicinity of ferroelectric domain walls allow the nucleation of conductive channels in the insulating material at temperature 10 K lower than T_{MI} of bulk VO_2 [101]. In this framework, it has been reported that VO_2 thin films exhibit phase coexistence on few K in the vicinity of T_{MI} with nanoscale metallic puddles appearing at the onset of the MIT [102]. Note also that a surface study of thin films of VO_2 grown on (110)-oriented substrates of rutile TiO_2 around T_{MI} and atmospheric pressure reports decoupled structural and electronic transitions and reveal the presence of an additional monoclinic-like metallic phase in between the M_1 and R phases [103]. Very recently, atomic resolution imaging and spectroscopy reveal the existence of fine-scale tweed structures on nm length scale in $VO_2/TiO_2(001)$ films [104]. Such textures, which behave like the standard metallic rutile phase, is in fact weaved by semi-dimerized chains of vanadium in a new monoclinic phase that appear to be a structural bridge between the different monoclinic insulating ground states of VO_2. These observations provide a multiscale perspective for the interpretation of existing data in thin films, where phase coexistence and structural intermixing occur down to atomic scale. Such patterns are controlled by the ferro-elastic nature of VO_2 and its response to misfit strain.

To finish two remarks can be done. Firstly, it is not clear if the observed phase separation reported in thin films is due to electron–electron repulsions in correlated materials or to elastic inhomogeneity in the films. Secondly, because of the key role of ferro-elasticity to achieve the texture of small-scale systems, one must be very careful before generalizing observation done in nano-systems to macroscopic VO_2.

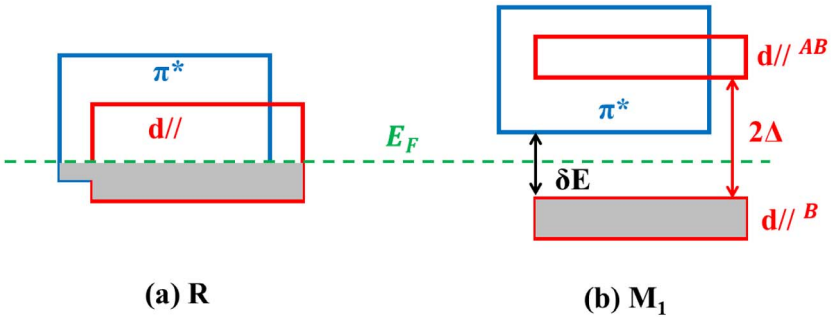

Figure 12. One electron representation of the electronic structure of (a) metallic and (b) insulating VO_2 according to [19]. δE is the optical gap between $d^{B}_{//}$ and π^* bands and 2Δ is the Peierls gap between $d^{B}_{//}$ and $d^{AB}_{//}$ bands.

4.3. *Beyond the Landau theory*

Renormalization group study of the critical behavior of the Ginzburg–Landau functional with a 4th degree polynomial expansion of the order parameter components allows us to determine, by the presence or absence of a stable fixed point, if the basic nature of the phase transition is of second order or of first order. These two possibilities occur for functionals with four-component order parameters. The order of the phase transition thus depends of the structure of the functional [105]. The analysis performed for the VO_2 functional shows the lack of a stable fixed point. Thus, according to [105], this finding is compatible with the experimental observation of a strong 1st order MIT in VO_2. Note that in this framework the first order nature of the MIT of VO_2 should be triggered by the sizeable pre-transitional structural fluctuations observed above T_{MI} (see Section 6).

5. Electronic structure of VO_2

The first convincing explanation of the MIT of VO_2, assuming a free electron picture, was proposed in the 1970's [19] by analyzing implicitly the influence of the two components of the M_1 vanadium shift on the metallic R band structure. This mechanism, which remains widely quoted nowadays, especially by experimentalists, is the main support at the so-called Peierls scenario of the MIT of VO_2. However as, since the 1970's, the description of the electronic structure of the insulating and metallic phases of VO_2 has been improved, Goodenough's scenario should be revisited. In this section we first recall Goodenough's model, then we present an up-to-date description of the electronic structure of metallic and insulating VO_2. As a lot of controversy remains in the literature on fine detail description, we concentrate our review on salient experimental and theoretical results for which there is an overall consensus.

5.1. *Model of Goodenough of the MIT*

The model starts from a simplified metallic band structure of VO_2. The V 3d levels are split by the oxygen octahedral crystalline field in such a way that the triplet of t_{2g} levels is well separated by ~2 eV from the doublet of highest energy e_g levels [106]. Thus, only the t_{2g} orbitals are occupied by the d^1 electron. Among them Goodenough distinguishes between the x^2–y^2 orbitals, in direct σ interaction along c_R (x direction), which gives rise to a quasi-1D $d_{//}$ band, and xy and yz orbitals,

in antibonding π interaction with triangular faces of the O octahedron, which gives rise to a quasi-isotropic set of π^* band (the t_{2g} orbitals are named according to the x, y, z octahedral setting of Figure 1a). One thus gets the schematic band structure of metallic VO_2 shown in Figure 12a, where the $d_{//}$ and π^* bands are partially filled by the V d^1 electron. In the following, it is useful for a better description of the electronic structure in the quasi-1D insulating phases, to differentiate the two types of π^* orbitals into xz orbitals, having a π-type bonding along c_R, and yz orbitals, having a δ-type bonding along c_R.

In order to describe the electronic change at the MIT, the individual V shift in the M_1 phase should be decomposed into two components, a zig-zag shift, u_z, towards one apical O and a dimerization shift, u_x, along c_R. There the V zig-zag shift u_z destabilizes the π^* levels by δE. This provokes an inter-band charge transfer from the π^* to the $d_{//}$ bands, the latter one becoming half-filled if δE is large enough. Assuming a half-filled quasi-1D $d_{//}$ band structure, the chain dimerization component u_x opens a Peierls gap 2Δ separating the bonding to the anti-bonding levels of the V–V dimer ($d^B_{//}$ and $d^{AB}_{//}$ respectively). With this double process M_1 becomes an insulator (semi-conductor) if δE is large enough so that the bottom energy of the π^* band is higher than the upper energy of the $d^B_{//}$ band, as shown in Figure 12b. δE measured at $\approx +0.68$ eV at ambient pressure [107, 108] supports this scenario. Note that in the opposite situation of negative δE, M_1 should remain metallic. It has been proposed that such a scenario could explain the metallization of pressurized VO_2 which keeps its M_1 structure [84].

Finally note that all these purely qualitative considerations are not based on a detailed energy balance between the electronic energy gain due to gap opening and the cost of lattice distortion energy. Also let us recall that the Peierls stabilizing mechanism requires a gap opening in a quasi-1D $d_{//}$ band. Electron–electron correlations are also ignored in this scenario. To conclude note that an unprecise denomination of the M_1 ground state is often done in the literature: a $2k_F$ Peierls ground state with one d electron per site ($2k_F = 1/2$ in chain reciprocal unit) does not corresponds to the establishment of a charge density wave (CDW) on the V site because all the V sites are structurally equivalent (see Figure 2), but to a bond order wave (BOW) where short bonds (those of the dimer) alternate with long bonds along c_R. To be more general note also that the V–V M_1 pairing can be described either by a $2k_F$ BOW Peierls pairing modulating the charge density of the bonds or by a spin-Peierls pairing of two neighboring spin 1/2 into a magnetic singlet on the dimer (see Section 5.3.2). As these two types of order are described by an order parameter of same symmetry (the amplitude of dimerization), one passes continuously from the Peierls limit to the spin-Peierls limit.

5.2. *Metallic phase*

5.2.1. *Quasi-isotropic electronic structure*

One fundamental assumption of Goodenough's scenario is the presence of a quasi-1D $d_{//}$ sub-band in the R phase of VO_2. It implies that a 1D electronic instability is an important aspect of the driving force of the MIT (this is the basis of the Peierls scenario). There is however no clear indication of a 1D anisotropy in the metallic structure. The electrical conductivity is quasi-isotropic between longitudinal (c_R) and transverse (a_R) directions: $\sigma_c/\sigma_a \sim 2.5$ [109]. Quasi-isotropy is also assessed by optically measured Drude plasma frequencies, $\Omega^c_P = 4.2$ eV and $\Omega^a_P = 3.56$ eV [110]. Moreover *ab-initio* band structure calculation shows that if the x^2–y^2 intrachain transfer integral is twice the xz and yz inter-chain transfer integrals [111], there are only two V coupled along c_R compared to 8 V inter-chain directions, see Figure 1a, so that the band structure should be relatively isotropic. This is sustained by the calculation [112] and measurements [113] of close Fermi surfaces. Also, the analogy between metallic VO_2 and transition metals like Pt or

Pd [24] where electrons in a comparatively wide π^* band screen out the interaction between the electrons in a narrow overlapping $d_{//}$ band is not really founded.

Finally let us remark that a recent angle-resolved photoemission (ARPES) investigation of VO_2 epitaxial thin film on $TiO_2(001)$ substrates (i.e., exhibiting an in-plane tensile strain induced by the lattice mismatch between the film and substrate—see Figure 10) provides evidence of 3 closed electron Fermi surface (FS) around the Γ point with one sub-FS exhibiting flat sections which could be nested by the $\mathbf{q}_R$ critical wave vector [113]. Also, an earlier electronic structure calculation evidences also a well-defined maximum of the electron–hole Lindhard response in metallic VO_2 at $\mathbf{q}_R$, which could be caused by some nesting of one sub-FS [112]. However, in all these cases, the $\mathbf{q}_R$ partial nesting should not be able to remove all the states at the Fermi level. At most, it could lead to a semi-metallic ground state and certainly not to a semi-conductor with the opening of the large gap experimentally observed. Also, it has not be established that partial nesting of the FS by a single $\mathbf{q}_R$ should lead to a minimum of free energy.

5.2.2. *Electron–electron correlations*

Magnetic measurements show that metallic VO_2 is a correlated metal. The spin susceptibility, χ_S, corresponds to an effective density of states at the Fermi level of $N_{\text{eff}}(E_F) \sim 10$ states/eV per VO_2 unit and spin direction [20,22]. With respect to a LDA density of states of $N(E_F) \sim 1.24$–1.31 states/eV per VO_2 unit and spin direction [33,114], χ_S presents a Stoner enhancement factor of 8. Also, a similar large enhancement factor of the linear coefficient γ of the thermal dependence of the electronic specific heat is found in low temperature metallic $V_{1-x}W_xO_2$ for $x = 0.14$ [23].

These experimental findings somewhat contrast with DMFT results where mapping of the spectral function on the self-energy of a Fermi-liquid leads to a weak mass renormalization: $m^*/m \approx 1.35$–1.8 [111,114,115], together with a still sizeable quasi-particle weight of $Z \sim 0.66$–0.50 [111,116]. Note that the finding of a negligeable mass enhancement ($m^*/m \sim 1$) and of a quasi-particle weight of $Z \sim 1/3$, in an earlier photoemission investigation of metallic VO_2 at 350 K [117], supports the description of VO_2 as a metal with an intermediate level of correlation. However, it is found that DMFT calculation of χ_S [114] and γ [116] disagrees by a factor 2–2.5 with the previously quoted experimental results.

The spectral function calculated by DMFT [111,116,118] in the R phase however bears some resemblance with that measured in more recent photoemission experiments. In the metallic phase the calculated spectral function exhibits a narrow quasiparticle coherence peak close to E_F together with two Hubbard bands: a weak lower Hubbard band (LHB) at about $-(1$–$1.5)$ eV below E_F and a stronger upper Hubbard band (UHB) at about $+(2$–$3)$ eV above E_F. The LHB has been detected in valence band photoemission spectra taken below E_F in the metallic phase just above the MIT [119]. However, it should be desirable to measure/calculate the spectral function at higher temperature when VO_2 behaves as a bad metal (see below).

The electrical resistivity increases as T in metallic VO_2 without saturation of the rate of increase at temperature as high as 840 K [120]. From conductivity and optical measurements an extremely short electron mean-free path comparable to c_R was deduced [120,121]. From this finding it was concluded that VO_2 is a bad metal. However, this interpretation rules out the standard quasiparticle picture of charge conduction in a Fermi liquid at high temperature. This is a clear indication that single site Coulomb repulsion energy (U) dominates the physics of metallic VO_2 [121]. Note however that a very short electron mean free path could be also due to the presence of a structural disorder caused, for example, by the onset of high temperature quasi-static lattice fluctuations announcing the MIT (see Section 6.4.1).

The previous analysis shows that VO_2 should be close to a Mott–Hubbard transition. More direct evidence of such an instability is provided by the study of $V_{1-x}Nb_xO_2$ solid solution. With x increasing the rutile unit cell volume sizably increases [55]. When x increases, until about

13.5% Nb, the spin susceptibility becomes significantly enhanced in a homogeneous manner (i.e., without no important local effect around the Nb impurity, which basically remains Nb^{4+} in the metal), while its thermal dependence progressively changes from a Stoner enhanced Pauli law to a Curie–Weiss law [20, 22]. For a Nb concentration, larger than $x_c \sim 20\%$ (for single crystal measurements), a metal non-metal electronic crossover keeping the R structure is observed [21, 55]. Interestingly, at this crossover concentration the c_R parameter reaches 2.93 Å [50, 55], which corresponds also to the repeat distance of V^{4+} zig-zag, with Mott–Hubbard localized electrons, in the M_2 phase. This metal nonmetal crossover occurring inside the R phase can be viewed as a Mott transition due to enhanced electron–electron correlations when, with the unit cell volume increase, the transfer integrals are reduced [62]. In the initial investigations it was suggested that the Mott–Hubbard charge localization could be also favored by an Anderson charge localization due to the Nb disorder with the onset of local effects around the Nb when approaching the insulating state [20]. However, charge localization due to dopant disorder is probably not very efficient because the R metallic state can be stabilized down to low temperature in Mo and W solid solutions (see Figure 7b) with an amount of dopant comparable to x_c at which the metal non-metal crossover is observed in $V_{1-x}Nb_xO_2$. Finally, note that cluster-DMFT calculations predicts a Mott–Hubbard metal–insulator transition inside the R phase of VO_2 for a one site Coulomb repulsion term U larger than 3–3.5 eV (see Figure 14 in [116]).

5.2.3. t_{2g} *orbital occupancy*

An important aspect of the MIT of VO_2 concerns the change of electronic anisotropy. While the electronic structure of the R metal is nearly isotropic, the insulating M_1 ground state exhibits a pronounced 1D electronic anisotropy with the formation of chains of V–V pairs. This anisotropy is experimentally assessed by the observation of a giant transfer of spectral weight at the MIT [119] together with an orbital occupation change from almost isotropic in R to almost completely σ polarized in M_1 [122]. It is thus desirable to characterize more precisely the influence of t_{2g} orbital degrees of freedom in the physical properties of metallic VO_2.

The t_{2g} orbital occupancy in metallic VO_2 has been probed by various experimental technics. A recent summary of the orbital occupancies experimentally determined and obtained from *ab-initio* calculations can be found in [44]. There is no real consensus on the results. Here we consider a recent determination [44] based on ^{51}V EFG measurements. Calculation of the experimental EFG on the V site is delicate because the EFG contains a contribution from all charges outside of the V and a contribution of the d^1 electron located inside the V sphere. In this latter contribution the d^1 electron occupies one of the 3 t_{2g} orbital states x^2–y^2, yz and xz in f_1, f_2 and f_3 proportion respectively (with $f_1 + f_2 + f_3 = 1$). The contribution of the d^1 electron at the EFG components on the V site can be expressed as [45]:

$$V_{xx} = -1.06(3f_2 - 1) \text{ a.u.} \tag{11}$$

$$V_{yy} = -1.06(3f_3 - 1) \text{ a.u.} \tag{12}$$

$$V_{zz} = -1.06(3f_1 - 1) \text{ a.u.} \tag{13}$$

These expressions are given in atomic unit (a.u.) which includes $\langle 1/r^3 \rangle$ calculated for a V^{4+}, according to the relation:

$$\frac{4}{7} e \left\langle \frac{1}{r^3} \right\rangle = -2.1 \text{ a.u.} \tag{14}$$

Note that residual e_g orbital occupancies contribute to f_1.

The thermal variation of the experimental EFG measured in the R phase is shown in Figure 13 (see also Table 1). By taking into account the calculated EFG due to surrounding ions, it is estimated by [44] a fractional t_{2g} orbital occupancy of $f_1 : f_2 : f_3 = 0.49(4) : 0.26(3) : 0.24(3)$ at

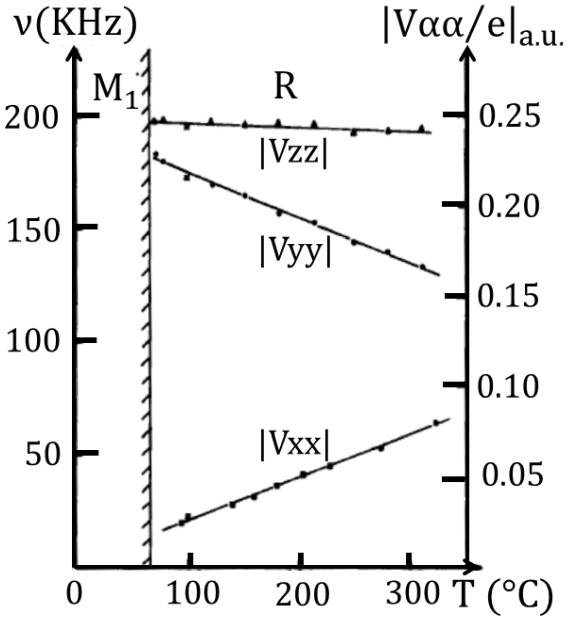

Figure 13. Thermal dependence of the modulus of the 3 principal components of the V^{51} electric field gradient tensor in metallic VO_2, expressed in the (x, y, z) frame of Figure 1a. The EFG is expressed in NMR frequency (KHz—left scale) and in atomic units (right scale) (adapted from [45]).

350 K. Note that soft-X-ray absorption spectroscopy at the V $L_{2,3}$ edges give a somewhat different occupancy ratio $f_1 : f_2 : f_3 = 0.33 : 0.51 : 0.16$ at 373 K [122].

However, the original information given by Figure 13 is that the EFG exhibits a sizeable thermal variation. This effect should be associated to a thermal variation of the fractional orbital occupancies f_i's of the d^1 electron inside the V sphere. More precisely, it was found that between 340 K and 585 K if f_1 stays nearly constant (it increases by 0.002 electrons) f_2 (f_3) increases (decreases) by 0.02 electrons. While the occupancy of the $d_{//}$ $(x^2–y^2) + e_g$ bands does not vary appreciably in temperature, an intra π^* band charge transfer from the yz orbitals to the xz orbitals occurs. As f_1 weakly decreases upon cooling it does not appear that the large decrease of the c_R parameter [34] stabilizes significantly the $d_{//}$ levels. This finding is difficult to reconcile with DMFT calculations predicting a sizeable variation of the $d_{//}$ partial density of states with c_R [116]. More interestingly, the decrease of occupancy of the yz orbitals which, by their δ overlap do not contribute to the bonding in V–V dimers of M_1, renders the electronic system more 1D on approaching the MIT. Such an effect is predicted in the so-called "Peierls-assisted orbital selection Mott instability" scenario of the MIT [115]. Consistently, the enhanced occupancy of π^* orbitals in the R phase of thin VO_2 (001) films (following the stabilization of yz orbitals due to the enhancement of V–O apical distances—see Figure 10) could provide a suitable explanation of the decrease of T_{MI} under uniaxial strain [81].

5.3. *Insulating phases*

5.3.1. V–V *dimer model of the* M_1 *phase*

The rich aspect of the phase diagram of VO_2 is the presence of different M_1, T and M_2 insulating ground states with very close free energy (Figures 8 and 9). Among these features a key

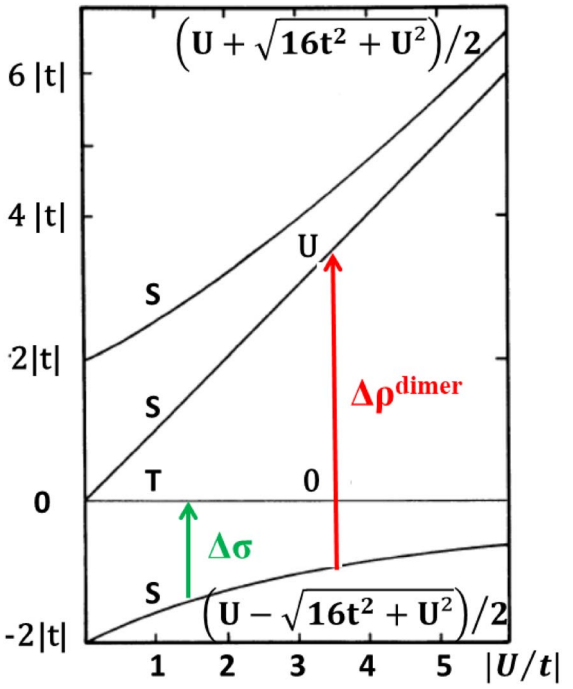

Figure 14. Energy levels of two electrons in the two-site Hubbard model with a hopping parameter t and an intra-atomic interaction U. The charge (singlet–singlet) and spin (singlet–triplet) excitations of the dimer, $\Delta\rho^{\text{dimer}}$ and $\Delta\sigma$ respectively, are shown (adapted from [38]).

observation is the finding of a Mott Hubbard localization of the d^1 electron in zig-zag V chains of the M_2 structure. This induces uniform $S = 1/2$ antiferromagnetic (AF) Heisenberg chains running along c_R whose magnetism is detected both by magnetic susceptibility [38] and ESR [123] measurements. Furthermore, the M_2 zig-zag chains continuously dimerize through the T phase to transform into V–V pairs of the M_1 phase (see Section 2.3). These magnetic features show that insulating M_1VO_2 cannot be considered as a conventional band semi-conductor as implied by Googenough's model (Figure 12b). With these magnetic results, it was suggested by [38] that the most realistic description of the M_1 electronic structure should start from a Heitler–London description of the electronic structure of V–V pair. The excitation spectrum of such a dimer is shown in Figure 14. This description was completed later by cluster DMFT calculations using the real M_1 structure [111]. Also, it was shown that the excitation spectrum of insulating M_1 simplifies to an effective band structure description [118, 124], whose excitations are basically those of the dimer excitation spectrum constructed on the eigenstates of the 2 electrons Hubbard molecule of Figure 14.

Enhanced electron–electron interactions cause a spin–charge separation. This manifests in the M_1 phase by the formation a gap of charge $\Delta\rho$ substantially larger than the gap of spin $\Delta\sigma$. The formation of different charge and spin excitations gaps is already contained in the excitation spectrum of the V dimer in the Heitler–London limit: $\Delta\rho^{\text{dimer}}$ and $\Delta\sigma$ in Figure 14. However, some caution must be taken in the interpretation of the experimental data because in addition to dimer excitation there are also excitation to additional π^* levels. In particular the empty π^* band is separated by an energy gap of $\delta E \approx 0.68$ eV from the $d^B_{//}$ filled levels which is significantly smaller than $\Delta\rho$ or $\Delta\rho^{\text{dimer}}$ [107, 108, 125]. When U/t of the dimer increases the charge excitation gap $\Delta\rho^{\text{dimer}}$ drastically evolves from the Peierls gap 2Δ between the $d^B_{//}$ and $d^{AB}_{//}$ electron states to a

gap of correlation of the order of U between the LHB and UHB. $\Delta\rho^{\text{dimer}}$, experimentally found at ~2.5 eV [107, 119, 126], is comparable to the intra-site Coulomb repulsion energy, U. In this limit the charge excitation spectrum should be nearly insensitive to the V shift change in the different insulating phases of VO_2. This is assessed by the observation of quite similar optical absorption spectra in the M_2, T and M_1 phases [127].

From the thermal dependence of the ^{51}V T_1 NMR relaxation rate in M_1, an activation energy corresponding to the spin gap or singlet–triplet energy of the V–V dimer, $\Delta\sigma \approx 0.24$ eV, can be deduced [128]. $\Delta\sigma$ is one order of magnitude less important than $\Delta\rho^{\text{dimer}}$. In contrast with the gap of charge, the gap of spin, $\Delta\sigma$, should crucially depend upon the V shift which progressively dimerizes the $S = 1/2$ AF Heisenberg chains formed in M_2, as we shall see below.

5.3.2. *Dimerization of the* M_2 $S = 1/2$ *AF Heisenberg chains and the* M_1 *spin-Peierls ground state*

In order to analyze the effect of V shift on the magnetic properties of the different insulating phases, let us generally describe the dimerized spin 1/2 AF Heisenberg chains by the 1D Hamiltonian:

$$H = 2\sum_{p}(J_1\mathbf{S}_{2\mathbf{p}}\cdot\mathbf{S}_{2\mathbf{p}+1} + J_2\mathbf{S}_{2\mathbf{p}+1}\cdot\mathbf{S}_{2\mathbf{p}+2}) \tag{15}$$

In (15), $\mathbf{S}_i$ is the spin 1/2 operator on site i, $J_1 = J\sqrt{\alpha}$ is the intra-dimer exchange interaction and $J_2 = J/\sqrt{\alpha}$ the inter-dimer exchange interaction. J is the exchange integral of the M_2 uniform Heisenberg chains. The amplitude of dimerization controls the $J_1/J_2 = \alpha > 1$ ratio of exchange interactions. The 1D nature of magnetic excitations is justified by the observation that in the M_2 (T) phase each zig-zag (weakly dimerized) chain is surrounded by 4 non-magnetic V paired chains (Figure 3).

Because of the Heisenberg chain dimerization in T, the uniform spin susceptibility measured in M_2 drops. This feature is characteristic of the M_2–T phase transition [38]. While the absolute value of the spin susceptibility in M_2 allows to determine J, the relative drop of spin susceptibility defines the spin gap $\Delta\sigma$. The reduced quantity $\Delta\sigma/J_1$ is tabulated in the literature [129–131] as a function of α. Figure 15a reports from magnetic measurements in $V_{1-x}Cr_xO_2$ for $x = 1\%$ [38] the variation of the spin gap in the T phase. This quantity is plotted in function of the V sublattice deformation parametrized by the EFG component V_{xx} of the V_1–V_1 pair.

Figures 15 reports the spin gap (a), the J_2/J_1 ratio (b) and J_1 (c) in the T phase. Another determination of the spin gap at ambient temperature in the T phase of stressed VO_2 can be obtained using the ^{51}V NMR linewidth broadening due to the short spin–lattice relaxation time T_1 of the dimerized zig-zag V sites [20]. These finding, which are also plotted in Figure 15, extend the $V_{1-x}Cr_xO_2$ results for T closer to the M_1 phase. By extrapolation of the data of Figure 15a to the M_1 phase, where $V_{xx} = 125$ KHz (see Table 1), one obtains a spin gap: $\Delta\sigma \approx 0.20 \pm 0.02$ eV (2300 ± 200 K). $\Delta\sigma$ is close to the activation energy, 0.24 eV, of the thermal dependence of T_1 measured in the M_1 phase of VO_2 [128]. However, a recent resonant inelastic X-ray scattering investigation has reported an excitation energy of 0.46 eV in this phase, which also has been attributed to the spin gap [125]. Some caution must be exercised because the magnetic excitation spectrum of dimerized or spin-Peierls (SP) systems is particularly subtle. In particular in the (weak coupling) RPA approximation, SP systems exhibit two excitation gaps at $\Delta\sigma$ and $2\Delta\sigma$ which link respectively the singlet ground state to a dispersing magnon branch and a two magnon continuum [132]. This two-gap structure has been detected by inelastic neutron scattering in the inorganic SP system $CuGeO_3$ [133] and in the organic SP system $(TMTTF)_2PF_6$ [134]. In this context it is possible that the spin gap of 0.46 eV in VO_2 could correspond to the excitation either towards the minimum of the continuum of two magnons [132] or towards a two magnon bound state of the dimerized chain [130].

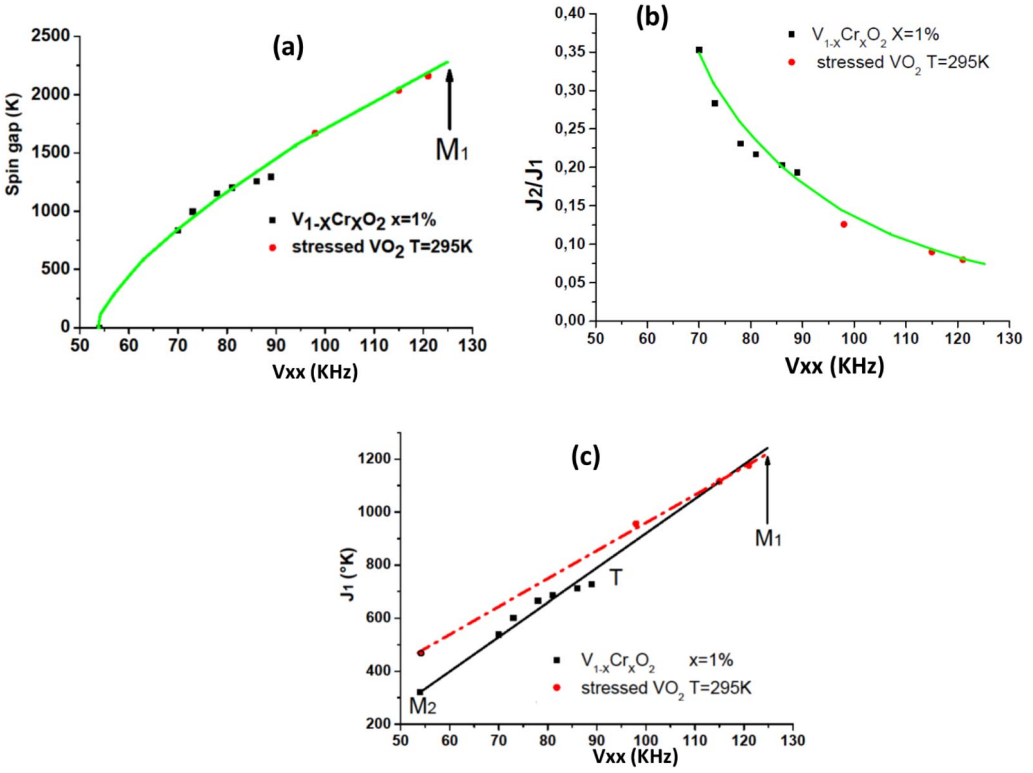

Figure 15. Spin gap $\Delta\sigma$ (a), J_2/J_1 ratio (b) and intra-dimer J_1 interaction (c) of the dimerized Heisenberg chain, modelized by (15), in the T phase of stressed VO_2 (red points) and of $V_{1-x}Cr_xO_2$ for $x = 1\%$ (black squares). These quantities are plotted in function of the smallest ^{51}V EFG component V_{xx} of the V_1–V_1 pairs. The correlation between V_{xx} and V_1–V_1/V_2–V_2 shortest distances in T is given in Figure 5a.

The extrapolation towards M_1 of other data shown in Figure 15 gives $J_1 \approx 1250$ K (Figure 15c) and $\alpha \approx 13$ (this inverse quantity is plotted in Figure 15b). The large α value means that, with $J_2 \sim 100$ K, V–V dimers are magnetically uncoupled in the M_1 phase. Consistently note that in this limit one has $\Delta\sigma \approx 2(J_1–J_2)$. Also, with a J_2 value as small as 100 K, it appears that the dimers should be decoupled by thermal fluctuations in the vicinity of T_{MI}. Thus, the analysis of magnetic properties in the M_1 phase of VO_2 using the isolated dimer limit is justified. This also justifies the use of an effective one particle potential [118, 124] and corroborates the Hubbard V–V dimer model of Figure 14.

The above analysis of magnetic measurements assumes that magnetic excitations remain 1D in all the insulating phases of VO_2. There is however no experimental information on the magnitude of the interchain exchange coupling $J_\perp$. But note that in the M_1 phase the anisotropy of exchange interaction $J_1/J_\perp$ should be greater than the J_1/J_2 ratio (for which $\alpha \approx 13$) because the V distance between neighboring dimers is smaller in chain direction (3.18 Å) than between chain (~3.5 Å) and the type of overlap of $d_{//}$ orbitals changes from σ to δ respectively.

Figure 15a shows that the spin gap $\Delta\sigma$ in the M_1 phase is much larger than J in the M_2 phase. Similarly, the intra-dimer exchange integral J_1 increases considerably by a factor 3 to 4 with respect to J during the T phase transformation. These variations should be associated to large variation of V–V intra-dimer distances (Figure 5a). Also, as J_1 and J_2 are sizably different of J,

the progressive dimerization of M_2 Heisenberg chains inside the T phase cannot be analyzed in the weak coupling limit. However, VO_2 with its 1st order M_2–T transition is quite different of "conventional" organic SP systems, such as TTF-CuBDT and MEM(TCNQ)$_2$, undergoing a 2nd order transition and, analyzed in the literature using a weak spin–lattice magnetoelastic interaction [135, 136]. Nevertheless, contrary to the assertions of [136], VO_2 remains the first SP system [38] clearly identified in the literature.

In VO_2, using a combination of Figures 5a and 15a, one finds that $\Delta\sigma$ increases nearly linearly when $\delta u = |d_T – d_{M_2}|$ increases (in this expression d_i is the difference of V_2–V_2 distances between dimerized Heisenberg chains in the T phase and zig-zag chains in the M_2 phase). From this linear plot one obtains a slope $g = \delta(\Delta\sigma)/\delta u$ of 0.54 eV per Å in VO_2. This slope is 3 times larger than $g = 0.18$ eV per Å found in the inorganic SP system $CuGeO_3$ and of $g = 0.14$–0.22 eV per Å for organic SP systems [137]. As the reduced spin–phonon coupling λ_{SP} entering in the theory of the SP transition is proportional to g^2 [135, 136], λ_{SP} of VO_2 should be one order of magnitude larger than λ_{SP} of "conventional" SP systems [135, 138]. The M_2 to T SP transition should thus be treated in the strong coupling limit. As conventional SP transitions, where λ_{SP} are smaller than 1, are of second order nature, the large λ_{SP} value could explain the first order nature of the M_2–T phase transition of VO_2. Finally note that the insulating M_1 phase has been previously analyzed in the literature [139] in the intermediate to strong coupling SP limit.

It is expected that a magnetic field, H, should lift the degeneracy of the V–V triplet level by Zeeman effect. As the spin gap $\Delta\sigma$ is quite large, it might be expected that a significant splitting could not be observed with available laboratory magnetic fields. However, the recent finding via optical means of a magnetic-field-induced insulator–metal transition in 6% W-doped VO_2 for an ultrahigh magnetic field of 500 T is a surprising result [140]. In this case it is not obvious that H should simply dissociate the M_1 V–V spin singlet by the Zeeman effect. The MIT mechanism should be more complex because a certain number of V–V dimers are already broken in W doped materials into V^{3+} W^{6+} entities by charge transfer from the dopant to the V [57]. Such a process is believed to be responsible of the large decrease of T_{MI} [62]. In addition, doping effect on the V–V insulating properties of VO_2 is certainly quite subtle because, in addition to the creation of pairing defects in the SP ground state, doping induces a V doping process which breaks the spin–charge decoupling by the creation of $S = 1$ V^{3+} entities. Note that such defects are different from the $S = 1/2$ charged decoupled solitons formed in SP disordered systems such as doped $CuGeO_3$ [141, 142]. Finally remark that low-frequency collective spin excitations have been recently detected in Raman spectra recorded in insulating phases of Mg doped VO_2 where $S = 0$ V^{5+} defects are created [143]. This mode has been identified as the breather (singlet spin excitation) mode of the SP chain interrupted by spin defects. These recent examples show that a systematic study of the influence of magnetic and charge defects on the physical properties of doped VO_2 should open a future important field of research which should be of greatest importance because of the use of doped VO_2 in the fabrication of devices.

6. Pre-transitional structural fluctuations in the metallic phase

6.1. *Criticality*

The R to M_1 structural transition is accompanied by the onset of superstructure Bragg reflections at the reduced critical wave vector $\mathbf{q}_R = (1/2, 0, 1/2)_R$ of the high temperature rutile Brillouin zone (Section 4.1). The onset of superstructure reflections at the equivalent reduced wave vector $\mathbf{q}_{R'} = (0, 1/2, 1/2)$ corresponds to the formation of another M_1 domain. These two critical wave vectors are shown in Figure 16. Also the R to M_1 structural instability gives rise to a pre-transitional X-ray diffuse scattering at $\mathbf{q}_R$ and $\mathbf{q}_{R'}$ reciprocal positions whose intensity $I(\mathbf{q}_R, T)$ behave critically

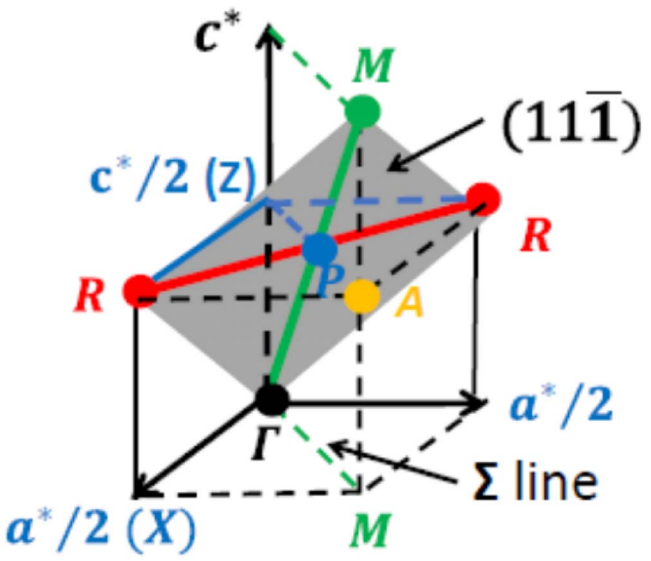

Figure 16. Rutile Brillouin zone showing two R critical points linked by the RPR rod (in red). This rod as well as the ΓPM line (in green), also indicated in Figure 19a, are located in the (11$\bar{1}$) layers in grey.

in function of the temperature [144]. More generally the diffuse scattering intensity $I(\mathbf{q}, T)$ measures, in addition to the squared structure factor of the lattice deformation, the Fourier transform $S(\mathbf{q}) = \langle|\mathbf{u}(\mathbf{q})|^2\rangle$ of the atomic (here the V) displacement–displacement correlation function $\langle\mathbf{u}(\mathbf{r})\mathbf{u}(\mathbf{r}')\rangle$. In the classical approximation (i.e., high temperature limit) one has the relationship:

$$\langle|u(\mathbf{q})|^2\rangle \propto k_B T \cdot \chi(\mathbf{q}) \tag{16}$$

where in the right member of (16) $\chi(\mathbf{q})$ is the real part of the generalized $\mathbf{q}$ susceptibility [145]. This susceptibility, associated to the order parameter of the structural transition (the amplitude of V shift) at $\mathbf{q}_R$, $\mathbf{u}(\mathbf{q}_R)$, should diverge at T_{MI} (or below T_{MI} for a 1st order phase transition). The inverse of this quantity $1/\chi(\mathbf{q}_R)$ which is proportional to $T/I(\mathbf{q}_R, T)$ generally decreases linearly in temperature, as expected from a Curie–Weiss dependence of $\chi(\mathbf{q}_R)$, and vanishes at the structural transition when this one is of 2nd order (because of the 1st order nature of MIT of VO_2 there is a small shift of the vanishing temperature of 10 K below T_{MI} in the data of [144]). This behaviour is outlined Figure 17.

To finish two important remarks must be made:

- In conventional X-ray diffuse scattering experiment the scattered intensity is integrated on all the energies, so the instantaneous correlation function $S(\mathbf{q}, t = 0)$ is in fact measured [145]. Also, contrarily to what is generally stated in the literature, the critical dependence of the diffuse scattering at structural transition does not bring any information concerning the critical dynamics of the phase transition. In particular the detection of a critical X-ray diffuse scattering is not the direct proof of the presence of a soft phonon mode. This aspect will be further developed in part 3.
- In addition to the detection of a critical behavior of the diffuse scattering in $\mathbf{q}_R$, pretransitional fluctuations can extend beyond $\mathbf{q}_R$ on a large $\mathbf{q}$ range in reciprocal space. Also, in many cases diffuse scattering method reveals anisotropic fluctuations in $\mathbf{q}$ [148]. Such fluctuations are those of a local order in real space whose, as stated previously,

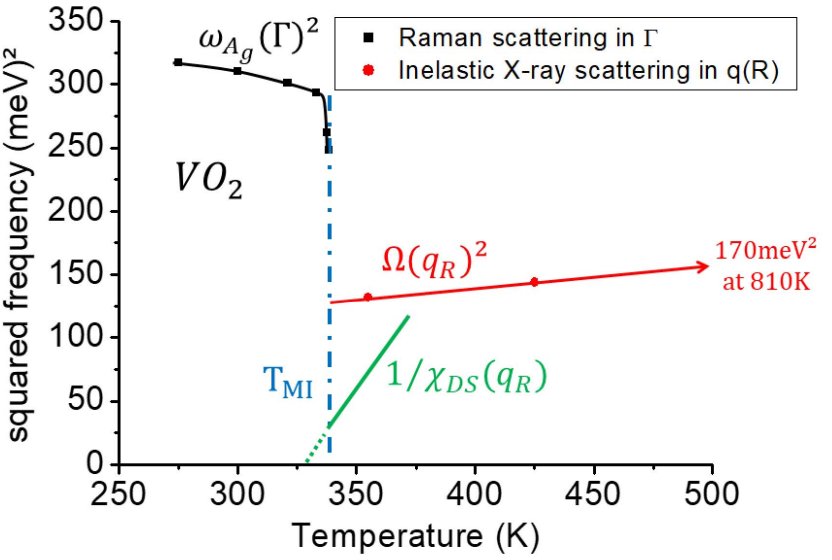

Figure 17. Thermal dependence of the squared frequency of the lowest frequency A_g Raman mode measured in Γ below T_{MI} [96, 146] and of the squared frequency of the lowest energy phonon measured in $\mathbf{q}_R$ above T_{MI} [147]. The thermal variation of this last quantity should be compared with $1/\chi_{DS}(\mathbf{q}_R)$ ($1/\chi(\mathbf{q}_R)$ in the text) obtained from the X-ray diffuse scattering measurements of [144]. $1/\chi_{DS}(\mathbf{q}_R)$ is expressed in arbitrary units.

dynamics is unknown. This local order announces the low temperature long range $\mathbf{q}_R$ order. Such a local order is due to structural correlations revealing a lattice instability. This point will be developed in part 2.

6.2. *Anisotropy*

6.2.1. *1D structural correlations*

Figure 18a presents an X-ray diffuse scattering pattern taken in the metallic phase of VO_2 at 345 K (T_{MI} + 5 K). It is obtained in close proximity of a section of the reciprocal space including the $[110]_R$ and $[001]_R$ directions. This X-ray pattern reveals two sets of oblique diffuse lines corresponding to the intersection of two families of {111} diffuse planes with the Ewald sphere (the section by the two others types of {111} diffuse planes give rise to broad circles that one can guess at large Bragg angles). A $(11\bar{1})$ reciprocal plane belonging to this family is drawn in the rutile Brillouin zone of Figure 16. It contains the R and R′ critical points of the MIT. The observed diffuse lines of Figure 18a are schematically represented in Figure 19a. These lines running along the ΓM direction, and its symmetry equivalent directions, do not contain the R point. It means that pre-transitional diffuse scattering has a much larger $\mathbf{q}$ extension than the $\mathbf{q}_R$ and $\mathbf{q}_{R'}$ critical wave vectors previously considered in part 1.

The presence of (111) and $(11\bar{1})$ planar diffuse scattering implies the existence of decoupled 1D correlated atomic displacement along the interpenetrating $[111]_R$ and $[11\bar{1}]_R$ directions which are located in the $(110)_R$ plane of the R structure shown in Figure 19b.

From the inspection of the experimental set of diffuse lines shown in Figure 18a, several observations can be done:

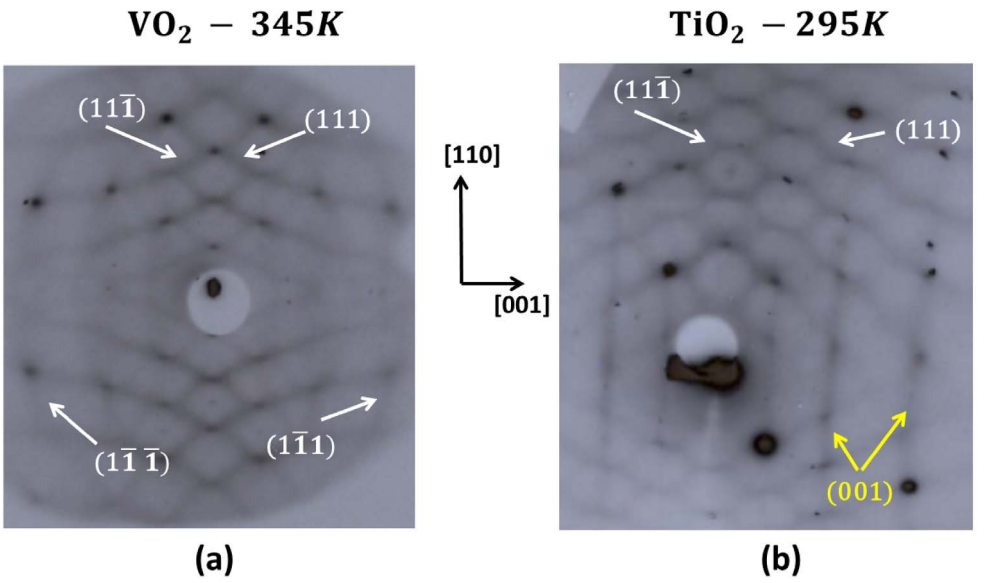

Figure 18. X-ray diffuse scattering pattern of VO_2 (a) and TiO_2 (b) in their rutile phase taken respectively with nearly the same crystal orientation by J. P. Pouget and R. Comès in the 1970–1975's. The reciprocal space orientation, close to the one represented in Figure 19a, is given in the figure. The different families of {111} diffuse lines are indicated by white arrows. The (001) diffuse lines, trace of ferroelectric correlations along c_R in TiO_2, are also indicated by yellow arrows.

- the presence of diffuse lines of continuous intensity means that the structure factor of the structural correlations originates from a well-defined atomic species (here the V). There is only an enhancement of intensity at the crossing point between different sets of diffuse lines.
- the absence of a diffuse line passing through the origin of the reciprocal lattice, together with the increase of diffuse scattering intensity along successive lines of the same set, imply a longitudinal shift of V in the $[111]_R$ direction perpendicular to each set of diffuse lines (see Figure 1b).
- as one diffuse line out of two is observed (Figure 19a), the atomic periodicity of the correlated V shift is one half of the $[111]_R$ periodicity. Thus, the shift of the two V of the rutile unit is in phase (Figure 19b).
- From the width along $[111]_R$ of a given diffuse line one deduces that the V longitudinal displacement is correlated on $\xi_{//} \approx 12$Å in the $[111]_R$ direction at $T_{MI} + 5$ K. This corresponds to 4 first neighbor V distances.

The above analysis, based on unpublished X-ray diffuse scattering data obtained in the 1970–1975's, perfectly agrees with the analysis recently published by [147]. An X-ray diffuse scattering pattern, resembling the one of Figure 18a, showing the same families of {111} planar pretransitional diffuse sheets, and taken in the R phase of the 10% Nb solid solution of VO_2, was previously published by [31].

Then two important remarks must be done:

- Firstly, diffuse lines perpendicular to the c_R direction expected from a Peierls/charge density wave or SP instability originating in the so-called quasi-1D $d_{//}$ sub-band structure of

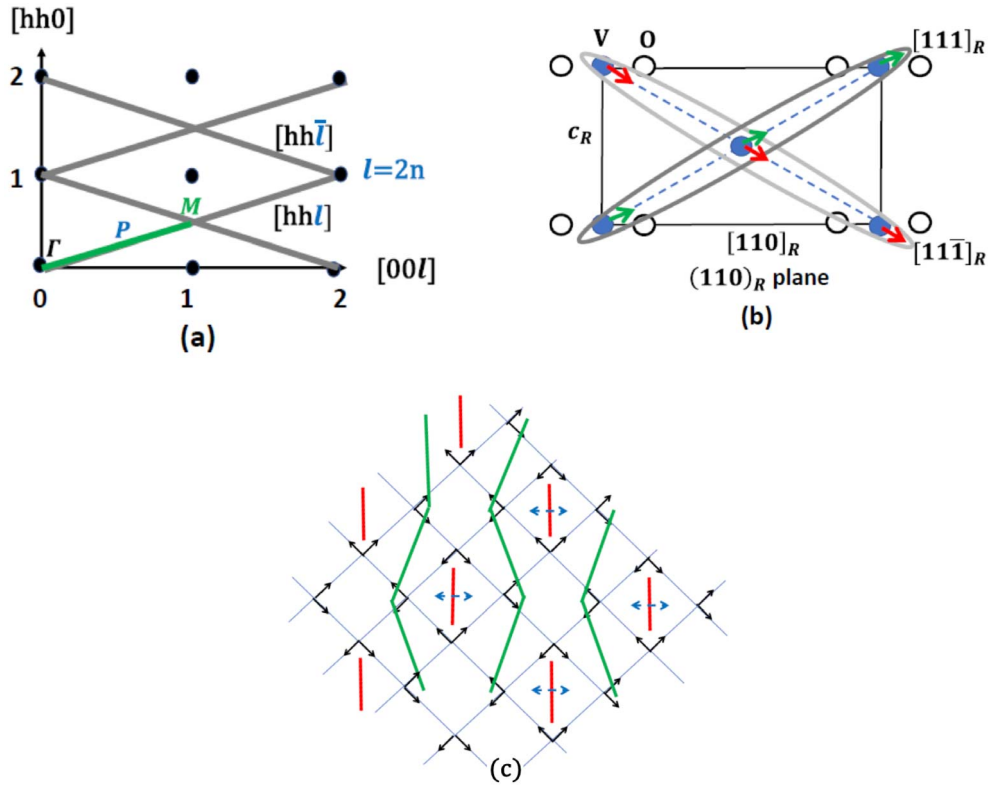

Figure 19. (a) Schematic representation of the two sets of diffuse lines observed on the X-ray patterns of Figure 18, together with their extinction condition. (b) Decoupled 1D longitudinal displacement of the V along the $[111]_R$ and $[11\bar{1}]_R$ rutile directions (in green and red respectively). (c) Coupling between the two sets of 1D V displacement of figure (b) giving rise to planar M_2-type atomic correlations with the formation of zig-zag V chains (green) and aligned V–V pairs (red). Steric repulsions between V pairing and V zig-zag are schematically indicated by blue arrows.

the R phase are not observed. The occurrence of 1D $2k_F$ fluctuations related to those instabilities is well documented in organic and inorganic systems [5].

- Secondly, the X-ray diffuse scattering pattern taken in the same orientation in rutile TiO_2 at ambient temperature, and shown in Figure 18b, is nearly identical to the one of VO_2 (Figure 18a). In particular, it exhibits the same kind of {111} set of diffuse sheets as VO_2. This finding was previously reported by [149]. However, the X-ray pattern of TiO_2 shown in Figure 18b reveals also an additional set of (001) diffuse planes, never reported, which corresponds to a Ti shift along the longitudinal c_R direction and correlated on $4c_R$ distances at 295 K. This diffuse scattering should be associated to an incipient ferroelectric instability of TiO_2 previously quoted in the literature [150]. Importantly, as TiO_2 is a d^0 band insulator, the diffuse scattering structured in {111} diffuse sheets should reveal an incipient structural instability of the rutile backbone. In this respect it is unlikely that the same type of $\langle 111\rangle_R$ correlated V displacements should correspond to an instability of the d^1 electron gas of VO_2.

Two additional observations support our analysis:

- EXAFS measurements reveal an anomalous increase of the Debye–Waller factors of atomic pairs in the $[111]_R$ and symmetry equivalent directions in the R phase [151]. However, these findings require a more elaborated interpretation because if there are 1D correlated V displacements along $[111]_R$, one expects, because of the 1D nature of the correlations, an enhanced disorder between V along interchain directions such as $[11\bar{1}]_R$ in Figure 19b.
- It has been established that characteristic spectral changes at the MIT of VO_2 films are observed down to a film thickness of 15 Å along c_R, and that smallest VO_2 films of less than 10 Å exhibit an insulating behavior without being V–V dimerized [152]. This finding could be related to the existence of the minimal correlation length of $\xi_{//} \approx 12$ Å along $[111]_R$ necessary to establish a local 1D structural order from which, by interchain coupling, the M_1V–V paired phase should nucleate (see next part).

Finally, note that the two X-ray patterns shown in Figure 18 reveal an additional feature. The set of {111} diffuse lines is slightly deformed at their crossing points, giving rise, especially for TiO_2, to a hexagonal shaped diffuse scattering. The precise origin of such a shaped diffuse scattering is not known. It could be caused by frustrated inter-chain interactions modifying the Fourier transform of the V displacement–displacement correlation function $\langle \mathbf{u}(\mathbf{r})\mathbf{u}(\mathbf{r}')\rangle$. Frustration could originate from the fact that in a $[110]_R$ plane each V is linked to six first V neighbors forming a deformed hexagon.

6.2.2. *2D structural correlations*

Coupling between V longitudinal positional fluctuations located on a lattice of interpenetrating chains, such as $[111]_R$ and $[11\bar{1}]_R$ chains shown in Figure 19b, should establish a phase relation between the V displacements at the crossing points of the two sets of chains. A phase shift between the different modulation waves which minimizes the interchain steric interactions is obtained for an out of phase V longitudinal displacement between first neighboring parallel chains. When superimposed with the V displacement pattern on the other equivalent set of parallel chains, one obtains the $(110)_R$ planar V correlations of M_2 type which is shown in Figure 19c. These V shift correlations define two sets of inequivalent chains running along c_R: zig-zag chains (in green in Figure 19c) located in between V–V paired chains (in red in Figure 19c). Note also that in Figure 19c the out of phase correlated zig-zag V displacement between first neighbor zig-zag chains along $[110]_R$ should modulate O–O octahedral distances in such a way that, in between the zig-zag chains, c_R chains of V–V pairs are localized in adjacent octahedra linked by the longest O–O edge. This is certainly V interactions via O displacements (i.e., octahedral deformation) which are at the origin of the interchain steric interactions outlined in blue in Figure 19c. The 3D lattice displacement pattern involved in the η_1 order parameter (Figure 4) is built with these planar steric correlations. Note that, similarly, the coupling between the two other directions of V displacement gives $(1\bar{1}0)_R$ planar correlations of M_2 type involved in the η_3 order parameter (Figure 4).

These 2D structural correlations should manifest by the presence of diffuse rods which should be located at the intersection of the (111) and $(11\bar{1})$ diffuse sheets. These diffuse rods (in red in Figure 16) join the R points of the Brillouin zone. Diffuse rods should intersect the ΓM diffuse scattering lines shown in Figure 18a at the P point (Figures 16 and 19a). Such a pattern of diffuse rods is not detected at $T_{MI} + 5$ K (Figure 18a). However, they are quite well observed in the insulating phase of $V_{1-x}Nb_xO_2$ for $x = 0.1$ [31] where they reveal the presence of a local M_2 order nucleated by the Nb disorder (see Section 3.1.1). Pre-transitional diffuse rods are detected in VO_2 in the diffractometry study of [144] only at $T_{MI} + 3$ K. These results mean that 2D structural correlations appears only few K above T_{MI}. In addition, critical fluctuations have been detected only in a 1 K temperature range above T_{MI} by the attenuation of longitudinal sound waves

coupled with the critical dynamics of the primary order parameter [153]. The critical exponent deduced from the thermal dependence of the attenuation can be accounted by the Landau theory of critical attenuation of an overdamped phonon with a 2D (rod-like?) dispersion in **q** space.

To summarize note that the critical scattering followed up to 400 K by [144] should be due to 1D structural fluctuations previously analyzed. The Curie Weiss behavior of the generalized susceptibility (Figure 17) reveals Gaussian fluctuations of the amplitude of the order parameter [5]. 2D structural fluctuations are detected only few K above T_{MI}. The intersection between different sets of [110] and $[\bar{1}10]$ diffuse rods occur at the R and R′ critical points. Thus, coupling between these 2D fluctuations should drive a 3D local order, precursor of the M_1 structural distortion. However, the critical regime of 3D fluctuations, which has not yet been reported, should be either extremely close to T_{MI}, or even hidden by the 1st order nature of the MIT.

According to the observation of high temperature structural chain-like correlations, we consider that the minimal ionic model allowing to analyze the structural instability of VO_2 should be 1D. This statement differs from a recent proposal of [154] considering that the minimal ionic Hamiltonian, which should involve strongest interactions between M_2 type of atomic displacements in either $(110)_R$ or $(1\bar{1}0)_R$ planes represented in Figure 4, should be 2D. Interestingly, this last work evokes the possibility of frustrated interactions between shifted V, which could be relevant for a deeper analysis of the X-ray diffuse scattering.

6.3. *Lattice dynamics at the MIT*

A general question related to structural transition concerns the possible existence of a critical phonon whose frequency softens on approaching the critical temperature T_C inside the high temperature phase. More precisely in the mean field scenario of a structural transition the square of the critical phonon frequency should vanishes proportionally to $(T-T_C)$ as does $1/\chi(\mathbf{q})$ for the critical wave vector [145]. Such a behavior is predicted in the weak coupling scenario of the Peierls transition [5] and experimentally verified in the case of the blue bronze, which is a typical Peierls system. In this compound it is observed the formation of a so-called $2k_F$ Kohn anomaly in the phonon spectrum [155, 156]. In the case of VO_2, the presence of a large incoherent nuclear cross section of the V renders phonon dispersion measurements not feasible using inelastic neutron scattering methods. Thus, speculations concerning the eventual presence of a $\mathbf{q}_R$ soft phonon which could drive the structural instability at the MIT of VO_2 came from first phonon spectrum calculations [157, 158].

Recently the situation has radically changed with the possibility to perform inelastic X-ray scattering measurements using synchrotron radiation. Recent measurements performed by [147] do not corroborate the scenario of a critical phonon frequency softening at the MIT of VO_2. The phonon of lowest frequency has an energy of $\Omega(\mathbf{q}_R) = 13$ meV at 810 K in the R phase. In addition, this frequency decreases only by 15% in a T range of 455 K on approaching T_{MI} and does not extrapolate at zero at finite temperature.

$\Omega(\mathbf{q}_R)$ measured in the metallic rutile phase has a frequency, ∼13 meV, smaller than the frequency of the Raman active modes measured in the insulating M_1 phase [146,159–163]. Among these Raman modes, the lowest energy mode, $\omega_{Ag}(\Gamma) = 18$ meV, exhibits an anomalous thermal variation. Its frequency softens only by 12%, but its damping increase sizably on approaching T_{MI} from below [96, 146]. This Raman response has an asymmetric shape with a Fano anti-resonance characteristic of the interaction of a phonon mode with a continuum of electron [163].

The "critical" $\omega_{Ag}(\Gamma)$ Raman mode measured in M_1 should correspond to $\Omega(\mathbf{q}_R)$ measured in the R phase. Figure 17 compares the thermal variation of the squared $\omega_{Ag}(\Gamma)^2$ Raman frequency with the squared $\Omega(\mathbf{q}_R)^2$ phonon frequency. None of these thermal dependencies is critical at T_{MI} (the critical behavior related to the development of a soft mode should lead to the vanishing

at $T_c \approx T_{MI}$ of these squared frequencies). Thus, the structural critical dynamics of the MIT of VO_2 does not follow the conventional displacive scenario implying the critical softening of a phonon mode as found for the Peierls transition in the blue bronze [155, 164]. Only $1/\chi_{DS}(\mathbf{q}_R)$ obtained from the X-ray diffuse scattering investigation and which integrates all the fluctuations in energy in the R phase behaves critically at T_{MI}. Thus, the critical dynamics of VO_2 should be more likely of the relaxational type, with the critical narrowing of a damped response centered at zero energy. In that case, the critical response is that of fluctuating local V clusters exhibiting the M_1 local structure and whose inverse lifetime corresponds to the energy damping of the quasi-static response. However, such a quasi-elastic critical response has not yet been measured in VO_2. But quasi-elastic 2D critical fluctuations (having the anisotropy of diffuse rods extending along the RPR reciprocal direction of the rutile Brillouin zone) have been measured by neutron scattering in the metallic rutile phase of the parent NbO_2 compound on approaching its MIT occurring at $T_{MI} \approx 1080$ K [165]. Note here that the critical wave vector of the MIT of NbO_2 is the P point of the Brillouin zone (see Figure 16) and not R as for VO_2.

The phonon spectrum of metallic VO_2 resembles that measured and calculated in insulating rutile TiO_2 [150]. The TiO_2 phonon spectrum exhibits low frequency modes at the M and R points of the Brillouin zone. The mode of lowest frequency at the M point is issued from a mixture between acoustic and optical phonon branches of the same Σ_1 symmetry. In TiO_2, the frequency of the optical branch drastically drops in the Σ direction from Γ (where it has the Γ_5^+ symmetry) to M [150]. A similar coupling between acoustic and optic branches occurs in VO_2, and the drastic frequency drop of this optical phonon branch along Σ appears be characteristic of the rutile structure [157]. Note that the M point which terminates the Σ line belongs to the {111} diffuse planes (see Figure 16). Also, the ΓR line of low frequency phonon in VO_2 belongs to these diffuse planes.

The lowest frequency phonon branch measured in metallic VO_2 is significantly damped, especially along the R–A–M direction [147]. Heavily damped zone center phonon modes are also found by Raman scattering in the R phase [159, 161, 163]. There, it has been suggested [163] that the broad Raman response of metallic VO_2 can be accounted by scattering process in strongly correlated materials. Also, phonon calculation which compares favorably with experimental results requires the inclusion of anharmonic effects [147, 166]. Differently, phonon spectrum calculation performed in the harmonic approximation gives, depending of the model, negative phonon frequencies (and thus an unstable lattice for these modulation wave vectors) in different points of the Brillouin zone [147, 158]. It is thus possible that the anharmonicity introduced in the calculation could mimic the propagation of phonons in a structure already including local quasi-static clusters of $[111]_R$ chains of correlated shifted V. A somewhat similar model have been used to analyze the anomalously broadened Raman phonon spectra of VO_2 [161].

In conclusion it appears that phonon anharmonicity and order–disorder type of critical dynamics, leading to clustering of locally shifted V in the metallic phase, are intimately related. Both features, associated with a strong electron–phonon coupling (see Section 7.2), could be taken as responsible for the non-development of a critical Kohn anomaly in the phonon spectrum.

6.4. *Chain-like order–disorder lattice instability*

6.4.1. *Generality and disorder amplitude*

X-ray diffuse scattering investigations reveal the presence in a large temperature range above T_{MI} of 1D interpenetrating lattices of quasi-static correlated longitudinal V displacements in $[111]_R$ and symmetry equivalent directions (Figure 19b). Figure 1b isolates a $[111]_R$ direction of V displacement in the rutile structure. It reveals that V shifts towards triangular octahedral faces

forming the ABAB type of compact packing of oxygen hexagonal layers in the rutile structure. This feature, which is also revealed by the X-ray diffuse scattering investigation of the rutile insulator TiO_2 (Figure 18b) could be a generic instability of the rutile structure. More generally, chain-like correlated atomic displacements are frequently observed in several classes of inorganic crystals [149]. In part b, below, we shall consider in detail the case of ferroelectric perovskites.

Analysis of the V Debye–Waller factor in the R metallic structure of VO_2 [34] found a quasi-isotropic root mean square (rms) V displacement of ~0.1 Å along each proper directions of the thermal ellipsoid. The magnitude of this rms displacement is comparable with V shift from the center of octahedra in the M_1 superstructure (see part 2.2). This provides an estimation of the magnitude of the quasi-static V shift disorder present in metallic VO_2. Electron scattering by this important quasi-static V disorder could efficiently contributes at the very short electron mean free path deduced by conductivity and optical measurements in metallic VO_2 [120, 121].

6.4.2. *Analogy with ferroelectric perovskites*

The X-ray diffuse scattering investigation of metallic VO_2 (see Section 6.2.1) reveals pre-transitional fluctuations consisting in uncoupled linear correlated V shifts away from the center of O octahedra, along the 4fold symmetry related diagonal $\langle 1,1,1\rangle_R$ directions of the rutile structure. Furthermore, the rutile diffuse scattering pattern shown in Figure 18, resembles the ones observed in $BaTiO_3$ and $KNbO_3$ ferroelectric perovskites [149,167]. These perovskites exhibit in their cubic (paraelectric) phase a set of {111} diffuse planes. This diffuse scattering is interpreted as due to pre-transitional uncoupled interpenetrating Ba/Nb linear displacements along the $\langle 1,1,1\rangle$ cubic directions. In ferroelectric perovskites, each 1D correlated Ba/Nb displacement induce a local polarization whose presence is at the origin of order–disorder models of ferroelectricity. In this case there are 8 site positions available for an off-center Ba/Nb displacement. This gives rise to the so-called "8-sites" order–disorder model of the literature [168]. There is however since several decades a controversy concerning the order–disorder or displacive origin of the critical dynamics of ferroelectric phase transitions in perovskites. However, the most recent investigations seem to comfort the "8-sites" model (see for example [169]).

6.4.3. *A possible order–disorder model*

The analogy with perovskite means that order–disorder type of 1D $\langle 1,1,1\rangle_R$ pre-transitional fluctuations in metallic VO_2 could be analyzed by a similar "8-sites" model. In such a model there are 8 possible shifts for each V (each shift from the site i being labelled by a generalized Ising variable σ_i with 8 components). In such a model V experiences an eightfold-well local potential sustaining an order–disorder type of dynamics. The microscopic justification of such a model could rely on the presence of a strong electron–phonon coupling (see Section 7.2). Note that a somewhat related "4-corner-sites" + "4-center-sites" model has been recently used to analyze V...V ionic coupling in the R phase of VO_2 [154]. In this analysis based on the presence of 2D M_2-type of V correlation (as shown in Figure 4) it is essential to separate center and corner V sites in the R structure, at the difference of $\langle 1,1,1\rangle_R$ 1D type of V correlation where such a distinction is not essential.

7. Structural contributions at the MIT of VO_2

7.1. *Incipient structural instability*

The MIT transition is preceded by an important thermal regime of $\langle 1,1,1\rangle_R$ 1D fluctuations in direct space revealed by the onset of {111} diffuse sheets in reciprocal space (part 6.2a). Also,

fluctuations of the 4-component order parameter are probably the cause of the 1st order nature of the MIT (see Section 4.3).

Such fluctuations, also observed in insulating TiO_2, are probably caused by an incipient instability of the rutile structure. Also, these anisotropic fluctuations cannot be related to a possible anisotropy of the electron-gas or to an eventual nesting process of the FS of VO_2, as it should be expected for a Peierls or CDW/BOW instability. In this framework, it is interesting to remark that in low dimensional metallic oxides and bronzes, such as the blue bronze $K_{0.3}MoO_3$ [156,170] or the monophosphate tungsten bronzes $(PO_2)_4(WO_3)_{2m}$ [171], the stabilization of a "$2k_F$" Peierls ground state uses also an incipient ferroelectric (case of the blue bronze) or antiferroelectric (case of the monophosphate tungsten bronze) instability of the oxide backbone. However, in these materials the Peierls transition is caused by an electron–hole electronic instability which uses the lattice ferroelectric/antiferroelectric incipient instability to be stabilized (i.e., the enhancement of the electron–phonon coupling due to the low frequency of these incipient phonon modes). This differs from VO_2 where, in spite of the fact that the underlying structural instability of the rutile structure seems to play a crucial role in the MIT through the stabilization of a M_2-type of order, the nature of its coupling to electronic degrees of freedom is not clear. Below, in Section 4 below, we shall propose a possible mechanism.

7.2. *Strong electron–phonon coupling?*

The MIT of VO_2 opens a quite large gap in the charge degrees of freedom accompanied by a sizeable V shift by about 0.2 Å, which forms V^{4+}–V^{4+} pairs. From this feature the presence of a large electron–phonon coupling (EPC) together with possible polaronic effects (see below) is expected. A large EPC is assessed by the detection of very broad phonon responses in Raman investigation of metallic VO_2 [159,161,163]. Although these features were noticed in the earlier time, there are only few theoretical treatments including the EPC on the same footing as electron–electron interactions in VO_2. Among them, except an earlier treatment by [172], only a recent theory combines DMFT with the adiabatic Born–Oppenheimer approximation [173]. This model includes electronic correlations, the multiorbital character of the electronic structure, and the two components of the antiferro-distortive mode (u_x and u_z defined in part 5.1). The model however separated u_x and u_z distortions. This assumption seems to be unrealistic because there is no possible decoupling between u_x and u_z components allowing obtaining the degenerated η order parameter (see Figure 4). Also, this model ignores that 1D pre-transitional fluctuations are not simply those of u_x and u_z, but a combination of these two components along the 4-equivalent $[111]_R$ directions. In addition, the theory assumes the adiabatic approximation.

An essential finding concerns the observation of order–disorder or relaxational dynamics for the structural counterpart of the MIT of VO_2, whose local order can be modeled by a "8-site" generalized Ising variable as for the ferroelectric perovskites (see Section 6.4.2). For a Peierls chain order–disorder or relaxational dynamics could be due to a strong electron–phonon coupling or to a non-adiabatic dynamic [5]. Note that an order disorder type of dynamics has been recently found in the Peierls system $BaVS_3$ [174]. The presence of a strong EPC is suggested by the detection of V displacement as large as 0.2 Å in the insulating phases. Various models of structural instability in metals undergoing a strong EPC are quite similar. As proposed by [175], the strong EPC can result via a polaronic capture mechanism between electrons and ions experiencing a double-well potential. In this model, applied to A15 superconductors, the local anharmonic potential is obtained via an interaction of electrons with a non-dispersive optical mode (Einstein mode). Here, the ion position between the two minima of a site i potential is described by an Ising variable σ_i. Then the ordering of ions in a lattice of double-well potential sites leads to a modulated electronic density. In this model there is similarity between the strong EPC limit of

the Peierls instability and the Jahn–Teller effect. Similar features are obtained in strongly EPC chain models developed by Aubry and coworkers (see for example [176]). In the model of [177], aiming to describe the CDW instability of metal dichalcogenides, an arbitrary ionic movement is analyzed and different contributions to the local elastic potential are explicitly evaluated. Strong EPC results in trapping the electron-cloud in the vicinity of an ionic site, leading to the creation of a double-well potential on each site i whose occupancy is specified by the Ising variable σ_i. Note that in this model the inter-site coupling between the σ_i's is due to the Ruderman–Kittel–Kasuya–Yosida (RKKY) interaction between the pseudo-spins which oscillates with the $2k_F$ momentum.

7.3. *Origin of the transition entropy*

Since the earlier studies of VO_2 has been a long-standing debate concerning the relative fraction of electronic and lattice component of the large entropy gain of $1.5k_B$ per VO_2 at the MIT. In these works, it was explicitly assumed that the dominant fraction at the transition entropy reveals the driving force of the transition. Various experimental and theoretical estimations can be found in Table I of [178]. In most of the determinations the phonon entropy is found to be dominant. However, the most recent experimental determinations remain controversial. In the work of [147], the variation of phonon entropy, ΔS^{ph}, at the R–M_1 transition is estimated at 68% of transition entropy while the work of [179], using the variation of Seebeck coefficients between R and M_1, the variation of electronic entropy, ΔS^{elec}, is estimated at 65% of transition entropy. The addition of these two determinations is 30% larger the experimental transition entropy.

These determinations however ignore the contribution of lattice fluctuations at the transition entropy which can be estimated from the X-ray diffuse scattering investigation in the R phase. Using a previous analysis performed in ferroelectric perovskites exhibiting similar sets of {111} diffuse sheets corresponding to correlated atomic displacements (on ξ) along $\langle 1,1,1\rangle$ cubic directions [180], the lattice fluctuation entropy can be simply estimated. In the "8-sites" model there are 2^3 possible shifts for the V. The entropy due to V disorder is thus:

$$S^{dis}/k_B = 3\ln 2. \tag{17}$$

With correlated V displacements on 4 sites ($\xi_{//} \approx 12$ Å) one obtains:

$$S^{fluct}/k_B = (3/4)\ln 2. \tag{18}$$

As O displacements are certainly correlated with V displacement, one gets $S^{fluct} = 0.52k_B$ per VO_2. This quantity is 1/3 of the total entropy of transition. Note that this value is two times smaller than the change of phonon entropy ΔS^{ph} estimated by [147]. S^{fluct} and ΔS^{ph} have different origin: S^{fluct} is due to the order–disorder nature of pre-transitional fluctuations, while ΔS^{ph} corresponds to the change of phonon spectra at T_{MI}. Finally note that $S^{fluct} + \Delta S^{elec}$ nicely amounts to the total entropy of transition of $1.5k_B$ per VO_2.

7.4. *What is really the mechanism of the MIT of* VO_2*?*

It is difficult to give a simple explanation of the MIT of VO_2 because there is no obvious continuity between metallic (R) and insulating (M_1) phases, due to the 1st order character of the transition. The absence of continuity is revealed by the fact that the electronic system in the rutile phase is multi-orbital and quasi-isotropic while the one of M_1 has a pronounced 1D character. As a consequence, there is a sizeable orbital charge transfer at the MIT. The metallic electron gas is described as moderately correlated, while electrons are localized in chains of V^{4+}–V^{4+} pairs

in M_1. There is also in this phase a sizeable spin–charge decoupling on the $d_{//}$ electronic subsystem so that the ground state can be described by a collection of magnetic singlet whose lower energy excitations, ~0.24 eV, those to the triplet state of the dimer, are one order of magnitude smaller than the gap of charge of the dimer of 2.8 eV which is comparable to U. In this respect the M_1 insulating ground state resembles more likely to the one of a spin-Peierls chain (exhibiting, as seen in Section 5.3.2, 1D magnetic excitations) with however the complication that the lowest charge excitation energy of 0.68 eV is the one towards π^* levels of different anisotropy and orbital symmetry than those, $d_{//}$, constituting the spin-Peierls system. Note that this confers a 3D degree of charge delocalization at the charge excitations, at the difference of the magnetic ones. Nevertheless, the important point is that there is an enhanced effect of electron–electron correlations at the MIT due to the reduction of dimensionality of the electron gas.

The mechanism of the MIT is variously described in the literature as Peierls, correlated Peierls or Mott–Hubbard type. These general concepts are only relevant to some salient features of the physics of VO_2, but not to the general specificity of the MIT. In our opinion the originality of the MIT of VO_2 is the change of electronic dimension from 3D to 1D which is not included in these general concepts. The Peierls transition occurs in quasi-1D electronic systems, while Mott–Hubbard localization occurs whatever the dimension of the electron gas. V–V pairing is typical of 1D physics while the spin–charge separation phenomenon, generally drives, in systems of higher electronic dimension, via a Mott–Hubbard transition, an antiferromagnetic ground state, as observed in V_2O_3 [7]. Very few systems undergo a MIT associated with a change of electronic dimension. To our knowledge there is another example among the 2D quarter filled organic conductor (BEDT-TTF)$_2$X series in which BEDT-TTF is bis-ethylenedithio-tetrathiafulvalene and X is a monovalent anion; for an introduction see [181]. Among them, θ-(BEDT-TTF)$_2$X 2D conducting salts with X = $RbZn(CN)_4$ or $RbCo(CN)_4$ undergoes a first order MIT at 200 K where, because of the shift of the BEDT-TTF due to the ordering of its terminal ethylene groups, the dimension of the electronic gas abruptly change from 2D to 1D [182]. Enhanced electron–electron correlations in reduced dimension thus drive a Mott–Hubbard charge localization of one hole per two BEDT-TTF, which stabilizes a charge ordered ground state below 200 K. Spin–charge decoupling in 1D systems induces the formation of spin 1/2 Heisenberg chains undergoing a spin-Peierls transition at ~25 K.

Another essential interaction in the physics of VO_2 is the EPC. It should be strong due to the presence of V shift of large amplitude in the insulating phases of VO_2. Such an interaction is essential in 1D systems to achieve a Peierls or a spin-Peierls ground state [5,136]. The presence of a strong EPC is assessed by Raman studies. Also, such a strong EPC could be taken as responsible of the absence of a phonon anomaly pre-transitional at the MIT.

The change of electronic dimension which favors electron localization phenomena responds, to the opinion of the author, at a structural instability inherent to the TiO_2-type rutile structure. This inherent instability is responsible of pre-transitional fluctuations consisting of correlated V 1D displacement along $\langle 1,1,1\rangle_R$ and symmetry equivalent directions on a large temperature range above T_{MI}. However, the MIT process appears to be really engaged only few K above T_{MI} when V displacements along different crossing chains are correlated in order to form a M_2 type of fluctuating 2D local order (Figure 19c). There, because of electron–electron repulsion a d^1 electron localizes on each V site of the uniform zig-zag chains. Also, because of steric interactions between V via the oxygen, Peierls or spin-Peierls V–V pairs of d^1 electrons are formed in between the zig-zag chains. Thus, one has half of the V sites are in the Mott–Hubbard ground state and the other half are in a singlet Peierls or spin-Peierls ground state. The formation of fluctuating insulating 2D M_2 clusters could be at the origin of the formation of a pseudo-gap ~1 K above T_{MI} [102]. The presence of a M_2-type instability inherent to pure VO_2 very close to T_{MI} is consistent

with the stabilization of the M_2 phase in modestly stressed VO_2 [77] and in strained VO_2 films [78, 79].

A specific aspect of the MIT of VO_2 is that the 3D interlayer local coupling stabilizing the M_1 3D order is not detected few K above T_{MI}. This offers the possibility for ultrafast spectroscopy experiments to bypass the MIT process by stabilizing metastable phases (see below). Also, the slow (relaxational) dynamics of the MIT, which manifests by a small energy response whose energy width can be estimated between ~4 meV in $BaVS_3$ [174] and half a meV in NbO_2 [165], should be an important temporal parameter of control of the MIT. With these considerations, VO_2 could be an excellent system for ultrafast spectroscopy investigations.

Ultrafast spectroscopy investigations have been recently reviewed by [183]. Thus, we summarize below only very salient results. Time-resolved synchrotron X-ray diffraction microscopy shows that the structural phase transformation in photo-excited VO_2 films is inhomogeneous on sub-micrometer length and sub-nanosecond time scales [184]. Inhomogeneity could result from nucleation of photoinduced nanometric metallic domains through the MIT [185]. Ultrafast spectroscopy provides evidence of a structural bottleneck timescale of 80 fs which corresponds to an energy cut off of the order of 10 meV [186]. Thus, it appears that the probe of coherent phonon modes whose energy is above this cut off limits the investigation of the MIT process [187]. Interestingly, pump-probe experiments on VO_2 films reveal the presence of nonequilibrium or non-thermodynamic transitory monoclinic metallic states between M_1 and R [188–190], which could resemble those observed by static measurements in thin films (see Section 4.2.3).

8. Concluding remarks

We have performed an exhaustive review of the physical properties of VO_2 putting in close relationship structural, electronic and magnetic investigations of this material and its alloys. After more than half a century of controversy on the nature of the MIT of VO_2, it appears now that electron–electron interactions play a decisive role and that the Peierls mechanism in a non-interacting electron gas, as originally formulated by Goodenough, is not sufficient to account the MIT. More elaborated scenarios have been proposed along this review. In particular the existence of an incipient structural instability triggering a change of electronic/orbital dimension are specific ingredient at the MIT of VO_2.

Superconductivity has not yet been reported in VO_2 [60]. However, it is interesting to remark that a superconducting dome extending up to 3 K inside an insulating phase, described as a "bipolaronic insulator", has been recently reported in epitaxial films of Ti_4O_7 [191]. Ti_4O_7, exhibiting pairing of Ti together with a subtle interplay between electron–electron and electron–phonon couplings [7], bears some similarities with VO_2. In Ti_4O_7 superconductivity occurs when the bipolaronic insulator is destroyed by charge doping. Thus, in this respect, it should be interesting to study more precisely the influence of charge injection on the physical properties of M_1VO_2, particularly at its phase boundary.

In spite of recent progress, many points remain to be clarified for the future. Among them important questions raised by this review concern:

- The role of substituents in the modification of the phase diagram of pure VO_2 (see Figure 6).
- The influence of charge and magnetic defects in the physical properties of VO_2 and its solid solutions.
- The phase diagram of VO_2 and its alloys under high pressure and high magnetic field.
- The influence of electron–phonon coupling, polaronic effects in the physics of VO_2 and its interplay with electron–electron correlations.
- A better characterization of the order–disorder dynamics in the mechanism of the MIT.

- The characterization of non-thermodynamic excited states during the 1st order MIT process.
- The role of structural disorder, of ferro-elasticity and of the formation of domain pattern for a better control of the MIT, particularly in strained films and derived devices.

Some general questions are not really specific to VO_2 since a wide class of correlated electronic systems undergo a MIT characterized by a strong interplay between charge, orbital and spin degrees of freedom subtly coupled to lattice degrees of freedom.

The mechanism of the MIT of VO_2 is quite complex, however we believe that it can be understood using in an appropriate manner physical concepts already established in the literature. In the opinion of the author, this transition seems to be quite unique among the other examples of MIT. This means that one can expect quite original applications of the physical and chemical properties of VO_2 to the design of various devices. A lot of performed world research is already focused on these developments. Future directions of research concerning potential applications of VO_2 are not explicitly mentioned in this review, but they were recently covered in the reviews of [27–30]. Also, understanding of physical and chemical processes involved in these applications should open new fundamental questions in material science.

Acknowledgements

My interest for VO_2 start in the 1970's with my thesis work, defended in 1974. During 1970–1976 I had frequent collaborations with chemists and physicists involved in the study of MIT. During this work, I particularly thank H. Launois, my thesis advisor, G. Villeneuve and M. Nygren on the chemistry side, P. Lederer and T. M. Rice on the theory side and R. Comès for his help in the X-ray diffuse scattering investigation of VO_2 during the 1975's. I thank also S. Biermann and A. Georges for recent discussions on the electronic structure of VO_2, and V. Balédent for a discussion on recent high-pressure experiments. Some of the new results developed in this review have been previously presented in a conference entitled "The metal–insulator transition of VO_2 revisited" at the symposium "Correlated electronic states in low dimensions" in honor of P. Lederer (Université Paris-Sud, France, 16–17 June 2008). Finally, I thank N. Mehl for her efficient bibliographic researches concerning references not easily traceable, J. Villain and T. Ziman for a critical reading of the manuscript.

References

[1] D. Adler, "Mechanisms for metal-nonmetal transitions in transition-metal oxides and sulfides", *Rev. Mod. Phys.* **40** (1968), p. 714-736.
[2] N. F. Mott, Z. Zinamon, "The metal-nonmetal transition", *Rep. Prog. Phys.* **33** (1970), p. 881-940.
[3] D. Adler, H. Brooks, "Theory of semiconductor-to-metal transitions", *Phys. Rev.* **155** (1967), p. 826-840.
[4] D. C. Mattis, W. D. Langer, "Role of phonons and band structure in metal-insulator phase transition", *Phys. Rev. Lett.* **25** (1970), p. 376-380.
[5] J. P. Pouget, "The Peierls instability and charge density wave in one-dimensional electronic conductors", *C. R. Phys.* **17** (2016), p. 332-356.
[6] Z. Zinamon, N. F. Mott, "Metal-non-metal transitions in narrow band materials; crystal structure versus correlation", *Philos. Mag.* **21** (1970), p. 881-895.
[7] M. Imada, A. Fujimori, Y. Tokura, "Metal-insulator transitions", *Rev. Mod. Phys.* **70** (1998), p. 1039-1263.
[8] D. I. Khomskii, *Transition Metal Compounds*, Cambridge University Press, Cambridge, 2014.
[9] N. Perrakis, "Contribution à l'étude de la magnéto-chimie du vanadium", *J. Phys. Radium* **8** (1927), p. 473-480.
[10] E. Hoschek, W. Klemm, "Weitere beitr age zur kenntnis der vanadinoxyde", *Z. Anorg. Allg. Chem.* **242** (1939), p. 63-69.
[11] O. A. Cook, "High-temperature heat contents of V_2O_3, V_2O_4, and V_2O_5", *J. Am. Chem. Soc.* **69** (1947), p. 331-333.
[12] F. J. Morin, "Oxides which show a metal-to-insulator transition at the Neel temperature", *Phys. Rev. Lett.* **3** (1959), p. 34-36.

[13] W. Rüdorff, G. Walter, J. Stadler, "Magnetismus, leitfähigkeit und reflexionsspektren von vanadindioxyd und vanadindioxyd-titandioxyd-mischkristallen", *Z. Anorg. Allg. Chem.* **297** (1958), p. 1-13.
[14] W. Westman, "Note on a phase transition in VO_2", *Acta Chem. Scand.* **15** (1961), p. 217.
[15] A. Magnéli, G. Andersson, "On the MoO_2 structure type", *Acta Chem. Scand.* **9** (1955), p. 1378-1381.
[16] G. Andersson, "Studies on vanadium oxides II. The crystal structure of vanadium dioxide", *Acta Chem. Scand.* **10** (1956), p. 623-628.
[17] K. Kosuge, "The phase transition in VO_2", *J. Phys. Soc. Japan* **22** (1967), p. 551-557.
[18] K. Kosuge, T. Takada, S. Kachi, "Phase diagram and magnetism of V_2O_3–V_2O_5 system", *J. Phys. Soc. Japan* **18** (1963), p. 318-319.
[19] J. B. Goodenough, "The two components of the crystallographic transition in VO_2", *J. Solid State Chem.* **3** (1971), p. 490-500.
[20] J. P. Pouget, H. Launois, "Metal-insulator phase transition in VO_2", *J. Phys. Colloq.* **37** (1976), p. C4-49-C4-57.
[21] G. Villeneuve, P. Hagenmuller, "Metal-insulator transitions in pure and doped VO_2", in *Localization and Metal-Insulator Transitions* (H. Fritzsche, D. Adler, eds.), Springer, Boston, MA, 1985, p. 39-52.
[22] J. P. Pouget, P. Lederer, D. S. Schreiber, H. Launois, D. Wohlleben, A. Casalot, G. Villeneuve, "Contribution to the study of the metal-insulator transition in the $V_{1-x}Nb_xO_2$ system: II Magnetic properties", *J. Phys. Chem. Solids* **33** (1972), p. 1961-1967.
[23] D. B. McWhan, J. P. Remeika, J. P. Maita, H. Okinaka, K. Kosuge, S. Kachi, "Heat capacity of vanadium oxides at low temperature", *Phys. Rev. B* **7** (1973), p. 326-332.
[24] A. Zylbersztejn, N. F. Mott, "Metal-insulator transition in vanadium dioxide", *Phys. Rev. B* **11** (1975), p. 4383-4395.
[25] R. M. Wentzcovitch, W. W. Schulz, P. B. Allen, "VO_2: Peierls or Mott–Hubbard? A view from band theory", *Phys. Rev. Lett.* **72** (1994), p. 3389-3391.
[26] T. M. Rice, H. Launois, J. P. Pouget, "Comment on "VO_2: Peierls or Mott–Hubbard? A View from Band Theory"", *Phys. Rev. Lett.* **73** (1994), article no. 3042.
[27] V. Devthade, S. Lee, "Synthesis of vanadium dioxide thin films and nanostructures", *J. Appl. Phys.* **128** (2020), article no. 231101.
[28] Y. Zhang, W. Xiong, W. Chen, Y. Zheng, "Recent progress on vanadium dioxide nanostructures and devices: fabrication, properties, applications and perspectives", *Nanomaterials* **11** (2021), article no. 338.
[29] K. Liu, S. Lee, O. Delaire, J. Wu, "Recent progress on physics and applications of vanadium dioxide", *Mater. Today* **21** (2018), p. 875-896.
[30] S. Shao, X. Cao, H. Luo, P. Jin, "Recent progress in the phase transition mechanism and modulation of vanadium dioxide materials", *NPG Asia Mater.* **10** (2018), p. 581-605.
[31] R. Comès, P. Felix, M. Lambert, G. Villeneuve, "Metal to insulator phase-transition in $V_{0,90}Nb_{0,10}O_2$ explained by local pairing of vanadium atoms", *Acta Cryst. A* **30** (1974), p. 55-60.
[32] Z. Hiroi, "Structural instability of the rutile compounds and its relevance to the metal-insulator transition of VO_2", *Prog. Solid State Chem.* **43** (2015), p. 47-69.
[33] V. Eyert, "The metal-insulator transitions of VO_2: A band theoretical approach", *Ann. Phys. (Leipzig)* **11** (2002), p. 650-702.
[34] D. B. Mc Whan, M. Marezio, J. P. Remeika, P. D. Dernier, "X-ray diffraction of metallic VO_2", *Phys. Rev. B* **14** (1974), p. 490-495.
[35] M. Marezio, D. B. Mcwhan, J. P. Remeika, P. D. Dernier, "Structural aspects of the metal-insulator transitions in Cr-doped VO_2", *Phys. Rev. B* **5** (1972), p. 2541-2551.
[36] J. M. Longo, P. Kierkegaard, "A Refinement of the Structure of VO_2", *Acta Chem. Scand.* **24** (1970), p. 420-426.
[37] G. Villeneuve, M. Drillon, P. Hagenmuller, "Contribution à l'étude structurale des phases $V_{1-x}Cr_xO_2$", *Mater. Res. Bull.* **8** (1973), p. 1111-1122.
[38] J. P. Pouget, H. Launois, T. M. Rice, P. Dernier, A. Gossard, G. Villeneuve, P. Hagenmuller, "Dimerization of a linear Heisenberg chain in the insulating phases of $V_{1-x}Cr_xO_2$", *Phys. Rev. B* **10** (1974), p. 1801-1815.
[39] M. Drillon, G. Villeneuve, "Diagramme de phase du système $V_{1-x}Al_xO_2$", *Mater. Res. Bull.* **9** (1974), p. 1199-1208.
[40] E. Pollert, G. Villeneuve, F. Ménil, P. Hagenmuller, "Le système $V_{1-x}Fe_xO_2$: propriétés structurales et magnétiques", *Mater. Res. Bull.* **11** (1976), p. 159-166.
[41] W. Brückner, U. Gerlach, W. Moldenhauer, H. P. Brückner, N. Mattern, H. Oppermann, E. Wolf, "Phase transitions and semiconductor-metal transition in $V_{1-x}Ga_xO_2$, single crystals", *Phys. Status Solidi (a)* **38** (1976), p. K13-K16.
[42] M. Ghedira, H. Vincent, M. Marezio, J. C. Launay, "Structural aspects of the metal-insulator transitions in $V_{0.985}Al_{0.015}O_2$", *J. Solid State Chem.* **22** (1977), p. 423-438.
[43] G. Villeneuve, M. Drillon, P. Hagenmuller, M. Nygren, J. P. Pouget, F. Carmona, P. Delhaes, "Magnetic and structural properties of stoichiometric and non-stoichiometric (V, Al) O_2 alloys", *J. Phys. C: Solid State Phys.* **10** (1977), p. 3621-3631.
[44] Y. Shimizu, T. Jin-no, F. Iwase, M. Itoh, Y. Ueda, "Occupation switching of d orbitals in vanadium dioxide probed via hyperfine interactions", *Phys. Rev. B* **101** (2020), article no. 245123.

[45] J. P. Pouget, "Etude par résonance magnétique nucléaire de la transition métal-isolant de VO_2 et ses alliages", PhD Thesis, Université Paris-Sud, France, 1974.

[46] J. Umeda, K. Narita, H. Kusumoto, "A study of magnetic resonance", *Hitachi Rev. (Japan)* **17** (1968), p. 204-211.

[47] J. Umeda, H. Kusumoto, K. Narita, "Nuclear magnetic resonance in polycrystalline VO_2", *J. Chem. Phys.* **42** (1965), p. 1458-1459.

[48] T. Hörlin, T. Niklewski, M. Nygren, "Electrical, magnetic and thermal studies of $V_{1-x}Ti_xO_2$ ($0 \le x \le 0.06$)", *Acta Chem. Scand. A* **30** (1976), p. 619-624.

[49] J. Umeda, S. Ashida, H. Kusumoto, K. Narita, "A new phase appearing in metal-semiconductor transition in VO_2", *J. Phys. Soc. Japan* **21** (1966), p. 1461-1462.

[50] W. Rüdorf, J. Märklin, "Die rutilphase $(V_{1-x}Nb_x)O_2$", *Z. Anorg. Allg. Chem.* **334** (1964), p. 142-149.

[51] H. Trarieux, J. C. Bernier, A. Michel, "Contribution à l'étude des systèmes VO_2–$NbVO_4$ et VO_2–$TaVO_4$", *Ann. Chim. (France)* **4** (1969), p. 183-194.

[52] C. N. R. Rao, M. Natarajan, G. V. Subba, R. E. Loehman, "Phase transitions and conductivity anomalies in solid solutions of VO_2 with TiO_2, NbO_2 and MoO_2", *J. Phys. Chem. Solids* **32** (1971), p. 1147-1150.

[53] T. Mitsuishi, "On the phase transformation of VO_2", *Japan J. Appl. Phys.* **6** (1967), p. 1060-1071.

[54] J. Galy, A. Casalot, J. Darriet, P. Hagenmuller, "Sur quelques nouvelles phases à caractère non-stæchiométrique dans les systèmes V_2O_5–VO_2–M_2O_3 (M:Al, Cr et Fe)", *Bull. Soc. Chim. France* **1** (1967), p. 227-234.

[55] G. Villeneuve, A. Bordet, A. Casalot, J. P. Pouget, H. Launois, P. Lederer, "Contribution to the study of the metal-insulator transition in the $V_{1-x}Nb_xO_2$ system: I—Crystallographic and Transport properties", *J. Phys. Chem. Solids* **33** (1972), p. 1953-1959.

[56] M. Nygren, M. Israelsson, "A D.T.A. study of the semiconductor-metallic transition in $V_{1-x}W_xO_2$, $0 \le x \le 0.067$", *Mater. Res. Bull.* **4** (1969), p. 881-887.

[57] T. Hörlin, T. Niklewski, M. Nygren, "Electrical and magnetic properties of $V_{1-x}W_xO_2$, $0 \le x \le 0.06$", *Mater. Res. Bull.* **7** (1972), p. 1515-1524.

[58] K. Shibuya, M. Kawasaki, Y. Tokura, "Metal-insulator transition in epitaxial $V_{1-x}W_xO_2$ ($0 \le x \le 0.33$) thin films", *Appl. Phys. Lett.* **96** (2010), article no. 022102.

[59] T. Hörlin, T. Niklewski, M. Nygren, "Electrical, magnetic and thermal studies on the $V_{1-x}Mo_xO_2$ system with $0 \le x \le 0.20$", *Mater. Res. Bull.* **8** (1973), p. 179-190.

[60] K. L. Holman, T. M. Mcqueen, A. J. Williams, T. Klimczuk, P. W. Stephens, H. W. Zandbergen, Q. Xu, F. Ronning, R. J. Cava, "Insulator to correlated metal transition in $V_{1-x}Mo_xO_2$", *Phys. Rev. B* **79** (2009), article no. 245114.

[61] O. Sävborg, M. Nygren, "Electrical, magnetic and thermal studies of the $V_{1-x}Re_xO_2$ system with $0 \le x \le 0.15$", *Phys. Status Solidi (a)* **43** (1977), p. 645-652.

[62] P. Lederer, H. Launois, J. P. Pouget, A. Casalot, G. Villeneuve, "Contribution to the study of the metal-insulator transition in the $V_{1-x}Nb_xO_2$ system: III—Theoretical discussion", *J. Phys. Chem. Solids* **33** (1972), p. 1969-1978.

[63] G. Villeneuve, "Transitions métal-isolant dans V1 − *x* Nb*x*O2 et V1 − *x* Crx O2 : aspects structuraux, magnétiques et électriques", PhD Thesis, Université de Bordeaux I, France, 1974.

[64] G. Villeneuve, A. Bordet, A. Casalot, P. Hagenmuller, "Propriétés physiques et structurales de la phase $Cr_xV_{1-x}O_2$", *Mater. Res. Bull.* **6** (1971), p. 119-130.

[65] E. Strelcov, A. Tselev, I. Ivanov, J. D. Budai, J. Zhang, J. Z. Tischler, I. Kravchenko, S. V. Kalinin, A. Kolmakov, "Doping-based stabilization of the M_2 phase in free-standing VO_2 nanostructures at room temperature", *Nano Lett.* **12** (2012), p. 6198-6205.

[66] K. Kosuge, S. Kachi, "Phase diagram of $V_{1-x}Fe_xO_2$ in the $0 \le x \le 0.25$ region", *Mater. Res. Bull.* **11** (1976), p. 255-262.

[67] W. Brückner, U. Gerlach, W. Moldenhauer, H. P. Brückner, B. Thuss *et al.*, "Metal-nonmetal transition in Fe and Al doped VO_2", *J. Phys. Colloq.* **37** (1976), p. C4-63-C4-68.

[68] W. Brückner, H. P. Brückner, U. Gerlach, B. Thuss, G. Fosterling, "The phase transition $M_1 \rightarrow T$ in $V_{1-x}Ga_xO_2$", *Phys. Status Solidi (a)* **38** (1976), p. 93-102.

[69] F. Pintchovski, W. S. Glaunsinger, A. Navrotsky, "Experimental study of the electronic and lattice contributions to the VO_2 transition", *J. Phys. Chem. Solids* **39** (1978), p. 941-949.

[70] Z. Hiroi, H. Hayamizu, T. Yoshida, Y. Muraoka, Y. Okamoto, J. Yamaura, K. Ueda, "Spinodal decomposition in the TiO_2–VO_2 system", *Chem Mater.* **25** (2013), p. 2202-2210.

[71] T. Hörlin, T. Niklewski, M. Nygren, "Vanadium-vanadium bonds in the $V_{1-x}Ti_xO_2$ system", *J. Phys. Colloq.* **37** (1976), p. C4-69-C4-73.

[72] M. Bayard, M. Pouchard, P. Hagenmuller, A. Wold, "Propriétés magnétiques et electriques de l'oxyfluorure de formule $VO_{2-x}F_x$", *Solid State Chem.* **12** (1975), p. 41-50.

[73] W. Brückner, U. Gerlach, H. P. Brückner, W. Moldenhauer, H. Oppermann, "Influence of non stoichiometry on the phase transitions in Ga-, Al-, and Fe-doped VO_2", *Phys. Status Solidi (a)* **42** (1977), p. 295-303.

[74] M. Bayard, M. Pouchard, P. Hagenmuller, "Propriétés structurales, magnétiques, et electriques de l'oxyfluorure $Cr_xV_{1-x}O_{2-x}F_x$", *Solid State Chem.* **12** (1975), p. 31-40.

[75] J. G. Ramirez, T. Saerbeck, S. Wang, J. Trastoy, M. Malnou, J. Lesueur *et al.*, "Effect of disorder on the metal-insulator transition of vanadium oxides: Local versus global effects", *Phys. Rev. B* **91** (2015), article no. 205123.
[76] D. Wickramaratne, N. Bernstein, I. I. Mazin, "Role of defects in the metal-insulator transition in VO_2 and V_2O_3", *Phys. Rev. B* **99** (2019), article no. 214103.
[77] J. P. Pouget, H. Launois, J. P. D'Haenens, P. Merenda, T. M. Rice, "Electron Localization Induced by Uniaxial Stress in Pure VO_2", *Phys. Rev. Lett.* **35** (1975), p. 873-875.
[78] J. H. Park, J. M. Coy, T. K. Kasirga, C. Huang, Z. Fei, S. Hunter, D. H. Cobden, "Measurement of a solid-state triple point at the metal-insulator transition of VO_2", *Nature* **500** (2013), p. 431-434.
[79] J. Cao, Y. Gu, W. Fan, L. Q. Chen, D. F. Ogletree, K. Chen *et al.*, "Extended mapping and exploration of the vanadium dioxide stress-temperature phase diagram", *Nano Lett.* **10** (2010), p. 2667-2673.
[80] J. M. Atkin, B. Berweger, E. K. Chavez, M. B. Raschke, J. Cao, W. Fan, J. Wu, "Strain and temperature dependence of the insulating phases of VO_2 near the metal-insulator transition", *Phys. Rev. B* **85** (2012), article no. 020101(R).
[81] N. B. Aetukuri, A. X. Gray, M. Drouard, M. Cossale, L. Gao, A. H. Reid *et al.*, "Control of the metal–insulator transition in vanadium dioxide by modifying orbital occupancy", *Nat. Phys.* **9** (2013), p. 661-666.
[82] Y. Muraoka, Y. Ueda, Z. Hiroi, "Large modification of the metal-insulator transition in strained VO_2 films grown on TiO_2 substrates", *J. Phys. Chem. Solids* **63** (2002), p. 965-967.
[83] Y. Chen, S. Zhang, F. Ke, C. Ko, S. Lee, K. Liu, B. Chen *et al.*, "Pressure—temperature phase diagram of vanadium dioxide", *Nano Lett.* **17** (2017), p. 2512-2516.
[84] E. Arcangeletti, L. Baldassarre, D. Di Castro, S. Lupi, L. Malavasi, C. Marini, A. Perucchi, P. Postorino, "Evidence of a pressure-induced metallization process in monoclinic VO_2", *Phys. Rev. Lett.* **98** (2007), article no. 196406.
[85] L. Bai, Q. Li, S. A. Corr, Y. Meng, C. Park, S. V. Sinogeikin, C. Ko, J. Wu, G. Shen, "Pressure-induced phase transitions and metallization in VO_2", *Phys. Rev. B* **91** (2015), article no. 104110.
[86] M. Mitrano, B. Maroni, C. Marini, M. Hanfland, B. Joseph, P. Postorino, L. Malavasi, "Anisotropic compression in the high-pressure regime of pure and chromium-doped vanadium dioxide", *Phys. Rev. B* **85** (2012), article no. 184108.
[87] V. Balédent, T. T. F. Cerqueira, R. Sarmiento-Pérez, A. Shukla, C. Bellin, M. Marsi, J.-P. Itié *et al.*, "High-pressure phases of VO_2 from the combination of Raman scattering and ab initio structural search", *Phys. Rev. B* **97** (2018), article no. 024107.
[88] J. R. Brews, "Symmetry considerations and the vanadium dioxide phase transition", *Phys. Rev. B* **1** (1970), p. 2557-2568.
[89] A. Tselev, I. A. Luk'yanchuk, I. N. Ivanov, J. D. Budai, J. Z. Tischler, E. Strelcov *et al.*, "Symmetry relationship and strain-induced transitions between insulating M_1 and M_2 and metallic R phases of vanadium dioxide", *Nano Lett.* **10** (2010), p. 4409-4416.
[90] Y. M. Gufan, V. P. Popov, "On the theory of phase transitions represented by four-component order parameters", *Sov. Phys. Crystallogr.* **25** (1980), p. 527-532.
[91] J. S. Kim, H. T. Stokes, D. M. Hatch, "Classification of continuous phase transitions and stable phases. II. Four-dimensional order parameters", *Phys. Rev. B* **33** (1986), p. 6210-6230.
[92] J. C. Toledano, P. Toledano, *The Landau Theory of Phase Transitions*, World Scientific, Singapore, 1987.
[93] M. Couzi, "On the Landau theory of structural phase transitions in layered perovskites $(CH_3NH_3)_2MCl_4$ (M = Mn, Cd, Fe): comparison with experiments", *J. Phys. I* **1** (1991), p. 743-758.
[94] J. C. Toledano, "La Ferroélasticité", *Ann. Telecom.* **29** (1974), p. 249-270.
[95] D. Maurer, A. Leue, R. Heichele, V. Müller, "Elastic behavior near the metal-insulator transition of VO_2", *Phys. Rev. B* **60** (1999), p. 13249-13252.
[96] P. Schilbe, D. Maurer, "Lattice dynamics in VO_2 near the metal-insulator transition", *Mater. Sci. Eng. A* **370** (2004), p. 449-452.
[97] J. C. Toledano, P. Toledano, "Order parameter symmetries and free-energy expansions for purely ferro-elastic transitions", *Phys. Rev. B* **21** (1980), p. 1139-1172.
[98] P. Toledano, J. C. Toledano, "Ferro-elastic transitions with a modification of the crystal's unit cell", *Ferroelectrics* **21** (1978), p. 587-588.
[99] P. J. Fillingham, "Domain structure and twinning in crystals of vanadium dioxides", *J. Appl. Phys.* **38** (1967), p. 4823-4829.
[100] A. Tselev, E. Strelcov, I. A. Luk'yanchuk, J. D. Budai, J. Z. Tischler, I. N. Ivanov *et al.*, "Interplay between Ferro-elastic and metal-insulator transitions in strained quasi-two-dimensional VO_2 nanoplatelets", *Nano Lett.* **10** (2010), p. 2003-2011.
[101] A. Tselev, V. Meunier, E. Strelcov, W. A. Shelton, I. A. Luk'yanchuk, K. Jones *et al.*, "Mesoscopic metal-insulator transition at Ferro-elastic domain walls in VO_2", *ACS Nano* **4** (2010), p. 4412-4419.
[102] M. M. Qazilbash, M. Brehm, B.-G. Chae, P.-C. Ho, G. O. Andreev, B.-J. Kim, S. J. Yun, A. V. Balatsky *et al.*, "Mott transition in VO_2 revealed by infrared spectroscopy and nano-imaging", *Science* **318** (2007), p. 1750-1753.
[103] J. Laverock, S. Kittiwatanakul, A. A. Zakharov, Y. R. Niu, B. Chen, S. A. Wolf, J. W. Lu, K. E. Smith, "Direct observation

of decoupled structural and electronic transitions and an ambient pressure monocliniclike metallic phase of VO_2", *Phys. Rev. Lett.* **113** (2014), article no. 216402.
[104] F. Sandiumenge, L. Rodríguez, M. Pruneda, C. Magén, J. Santiso, G. Catalan, "Metallic diluted dimerization in VO_2 tweeds", *Adv. Mater.* **33** (2021), article no. 2004374.
[105] J. C. Toledano, L. Michel, P. Toledano, E. Brézin, "Renormalization-group study of fixed points and of their stability for phase transitions with four-component order parameters", *Phys. Rev. B* **31** (1985), p. 7171-7196.
[106] C. Sommers, R. de Groot, D. Kaplan, A. Zylbersztejn, "Cluster calculations of the electronic d-states in VO_2", *J. Phys. Lett.* **36** (1975), p. L-157-L-160.
[107] S. Shin, S. Suga, M. Taniguchi, M. Fujisawa, H. Kanzaki, A. Fujimori *et al.*, "Vacuum-ultraviolet reflectance and photoemission study of the metal-insulator phase transitions in VO_2, V_6O_{13} and V_2O_3", *Phys. Rev. B* **41** (1990), p. 4993-5009.
[108] T. Peterseim, M. Dressel, M. Dietrich, A. Polity, "Optical properties of VO_2 films at the phase transition: influence of substrate and electronic correlations", *J. Appl. Phys.* **120** (2016), article no. 075102.
[109] P. F. Bongers, "Anisotropy of the electrical conductivity in VO_2 single crystals", *Solid State Commun.* **3** (1965), p. 275-277.
[110] H. W. Verleur, A. S. Barker, C. N. Berglund, "Optical Properties of VO_2 between 0.25 and 5 eV", *Phys. Rev.* **172** (1968), p. 788-798.
[111] S. Biermann, A. Poteryaev, A. I. Lichtenstein, A. Georges, "Dynamical singlets and correlation-assisted Peierls transition in VO_2", *Phys. Rev. Lett.* **94** (2005), article no. 026404.
[112] M. Gupta, A. J. Freeman, D. E. Ellis, "Electronic structure and lattice instability of metallic VO_2", *Phys. Rev. B* **16** (1977), p. 3338-3351.
[113] Y. Muraoka, H. Hiroki, Y. Yao, T. Wakita, K. Terashima, T. Yokoya, H. Kumigashira, M. Oshima, "Fermi surface topology in a metallic phase of VO_2 thin films grown on TiO_2 (001) substrates", *Sci. Rep.* **8** (2018), article no. 17906.
[114] A. Belozerov, A. Poteryaev, V. Anisimov, "Evidence for strong Coulomb correlations in the metallic phase of vanadium dioxide", *JETP Lett.* **93** (2011), p. 70-74.
[115] C. Weber, D. O. O'Regan, N. D. M. Hine, M. C. Payne, G. Kotliar, P. B. Littlewood, "Vanadium dioxide: A Peierls–Mott insulator stable against disorder", *Phys. Rev. Lett.* **108** (2012), article no. 256402.
[116] B. Lazarovits, K. Kim, K. Haule, G. Kotliar, "Effects of strain on the electronic structure of VO_2", *Phys. Rev. B* **81** (2010), article no. 115117.
[117] K. Okazaki, H. Wadati, A. Fujimori, M. Onoda, Y. Muraoka, Z. Hiroi, "Photoemission study of the metal-insulator transition in VO_2/TiO_2 (001): Evidence for strong electron-electron and electron-phonon interaction", *Phys. Rev. B* **69** (2004), article no. 165104.
[118] J. M. Tomczak, F. Aryasetiawan, S. Biermann, "Effective band structure in the insulating phase versus strong dynamical correlations in metallic VO_2", *Phys. Rev. B* **78** (2008), article no. 115103.
[119] T. C. Koethe, Z. Hu, M. W. Haverkort, C. Schüßler-Langeheine, F. Venturini, N. B. Brookes *et al.*, "Transfer of spectral weight and symmetry across the metal-insulator transition in VO_2", *Phys. Rev. Lett.* **97** (2006), article no. 116402.
[120] P. B. Allen, R. M. Wentzcovitch, W. W. Schulz, P. C. Canfield, "Resistivity of the high temperature metallic phase of VO_2", *Phys. Rev. B* **48** (1993), p. 4359-4363.
[121] M. M. Qazilbash, K. S. Burch, D. Whisler, D. Shrekenhamer, B. G. Chae, H. T. Kim, D. N. Basov, "Correlated metallic state of vanadium dioxide", *Phys. Rev. B* **74** (2006), article no. 205118.
[122] M. W. Haverkort, Z. Hu, A. Tanaka, W. Reichelt, S. V. Streltsov, M. A. Korotin *et al.*, "Orbital-assisted metal-insulator transition in VO_2", *Phys. Rev. Lett.* **95** (2005), article no. 196404.
[123] J. P. D'Haenens, D. Kaplan, P. Meranda, "Electron spin resonance in $V_{1-x}Cr_xO_2$", *J. Phys. C: Solid State Phys.* **8** (1975), p. 2267-2273.
[124] J. M. Tomczak, S. Biermann, "Effective band structure of correlated materials: the case of VO_2", *J. Phys.: Condens. Matter* **19** (2007), article no. 365206.
[125] H. He, A. X. Gray, P. Granitzka, J. W. Jeong, N. P. Aetukuri, R. Kukreja, L. Miao, S. A. Breitweiser *et al.*, "Measurement of collective excitations in VO_2 by resonant inelastic x-ray scattering", *Phys. Rev.* **94** (2016), article no. 161119(R).
[126] M. M. Qazilbash, A. A. Schafgans, K. S. Burch, S. J. Yun, B. G. Chae, B. J. Kim, H. T. Kim, D. N. Basov, "Electrodynamics of the vanadium oxides VO_2 and V_2O_3", *Phys. Rev. B* **77** (2008), article no. 115121.
[127] T. J. Huffman, C. Hendriks, E. J. Walter, J. Yoon, H. Ju, R. Smith, G. L. Carr, H. Krakauer, M. M. Qazilbash, "Insulating phases of vanadium dioxide are Mott–Hubbard insulators", *Phys. Rev. B* **95** (2017), article no. 075125.
[128] K. Takanashi, H. Yasuoka, Y. Ueda, K. Kosuge, "NMR studies of VO_2 and $V_{1-x}W_xO_2$", *J. Phys. Soc. Japan* **52** (1983), p. 3953-3959.
[129] L. N. Bulaevskii, "Magnetic susceptibility of a chain of spins with antiferromagnetic interaction", *Sov. Phys. Solid State* **11** (1969), p. 921-924 (*Fiz. Tverd. Tela* **11**, 1132).
[130] T. Barnes, J. Riera, D. A. Tennant, "$S = 1/2$ alternating chain using multi-precision methods", *Phys. Rev. B* **59** (1999), p. 11384-11397.
[131] D. C. Johnston, R. K. Kremer, M. Troyer, X. Wang, A. Klümper, S. L. Bud'ko, A. F. Panchula, P. C. Canfield, "Thermo-

dynamics of spin $S = 1/2$ antiferromagnetic uniform and alternating-exchange Heisenberg chains", *Phys. Rev. B* **61** (2000), p. 9558-9606.

[132] G. S. Uhrig, H. J. Schulz, "Magnetic excitation spectrum of dimerized antiferromagnetic chains", *Phys. Rev. B* **54** (1996), p. 9624-9627(R).

[133] M. Aïn, J. E. Lorenzo, L. P. Regnault, G. Dhalenne, A. Revcolevschi, B. Hennion, T. Jolicoeur, "Double gap and solitonic excitations in the spin-Peierls chain $CuGeO_3$", *Phys. Rev. Lett.* **78** (1997), p. 1560-1963.

[134] J. P. Pouget, P. Foury-Leylekian, S. Petit, B. Hennion, C. Coulon, C. Bourbonnais, "Inelastic neutron scattering investigation of magnetostructural excitations in the spin-Peierls organic system $(TMTTF)_2PF_6$", *Phys. Rev. B* **96** (2017), article no. 035127.

[135] A. I. Buzdin, L. N. Bulaevskii, "Spin–Peierls transition in quasi-one-dimensional crystals", *Usp. Fiz. Nauk* **131** (1980), p. 495-510.

[136] J. W. Bray, L. V. Interrante, I. S. Jacobs, J. C. Bonner, "The spin-Peierls transition", in *Extended Linear Chain Compounds* (J. S. Miller, ed.), vol. 3, Plenum Publishing Coorporation, 1983, p. 353-415.

[137] O. Jeannin, E. W. Reinheimer, P. Foury-Leylekian, J.-P. Pouget, P. Auban-Senzier, E. Trzop, E. Collet, M. Fourmigué, "Decoupling anion-ordering and spin-Peierls transitions in a strongly one-dimensional organic conductor with a chessboard structure, $(o\text{-}Me_2TTF)_2NO_3$", *IUCrJ* **5** (2018), p. 361-372.

[138] J. P. Pouget, "Microscopic interactions in $CuGeO_3$ and organic Spin-Peierls systems deduced from their pre-transitional lattice fluctuations", *Eur. Phys. J. B* **20** (2001), p. 321-333, *Eur. Phys. J. B*, **24**, 415.

[139] J. Shi, R. Bruinsma, A. R. Bishop, "Theory of vanadium dioxide", *Synth. Met.* **41–43** (1991), p. 3527-3530.

[140] Y. H. Matsuda, D. Nakamura, A. Ikeda, S. Takeyama, Y. Suga, H. Nakahara, Y. Muraoka, "Magnetic-field-induced insulator–metal transition in W-doped VO_2 at 500 T", *Nat. Commun.* **11** (2020), article no. 3591.

[141] B. Grenier, J.-P. Renard, P. Veillet, C. Paulsen, R. Calemczuk, G. Dhalenne, A. Revcolevschi, "Magnetic susceptibility and phase diagram of $CuGe_{1-x}Si_xO_3$ single crystals", *Phys. Rev. B* **57** (1998), p. 3444-3453.

[142] J.-P. Pouget, S. Ravy, J. P. Schoeffel, G. Dhalenne, A. Revcolevschi, "Spin-Peierls lattice fluctuations and disorders in CuGeO3 and its solid solutions", *Eur. Phys. J. B* **38** (2004), p. 581-598.

[143] R. Basu, V. Srihari, M. Sardar, S. K. Srivastava, S. Bera, S. Dhara, "Probing phase transition in VO_2 with the novel observation of low-frequency collective spin excitation", *Sci. Rep.* **10** (2020), article no. 1977.

[144] H. Terauchi, J. B. Cohen, "Diffuse x-ray scattering due to the lattice instability near the metal-semiconductor transition in VO_2", *Phys. Rev. B* **17** (1978), p. 2494-2496.

[145] J. P. Pouget, "Structural instabilities", in *Highly Conducting Quasi-One-Dimensional Organic Crystals, chapter 3* (E. Comwell, ed.), Semiconductors and Semimetals, vol. 27, Academic Press Inc., 1988, p. 87-214.

[146] R. R. Andronenko, I. N. Goncharuk, V. Y. Davydov, F. A. Chudnovskii, E. B. Shadrin, "Direct observation of the soft mode at a semiconductor-metal phase transition in vanadium dioxide", *Phys. Solid State* **36** (1994), p. 1136-1139.

[147] J. D. Budai, J. Hong, M. E. Manley, E. D. Specht, C. D. Li, J. Z. Tischler *et al.*, "Metallization of vanadium dioxide driven by large phonon entropy", *Nature* **515** (2014), p. 535-539.

[148] J. P. Pouget, A. M. Levelut, J. F. Sadoc, "André Guinier: Local order in condensed matter", *C. R. Phys.* **20** (2019), p. 725-745.

[149] R. Comès, M. Lambert, A. Guinier, "Désordre Linéaire dans les Cristaux (cas du Silicium, du Quartz, et des Pérovskites Ferroélectriques)", *Acta Cryst. A* **26** (1970), p. 244-254.

[150] J. G. Traylor, H. G. Smith, R. M. Nicklow, M. K. Wilkinson, "Lattice dynamics of rutile", *Phys. Rev. B* **3** (1971), p. 3457-3472.

[151] I.-H. Hwang, Z. Jin, C.-I. Park, S.-W. Han, "The influence of structural disorder and phonon on metal-to-insulator transition of VO_2", *Sci. Rep.* **7** (2017), article no. 14802.

[152] D. Shiga, B. E. Yang, N. Hasegawa, T. Kanda, R. Tokunaga, K. Yoshimatsu, R. Yukawa, M. Kitamura, K. Horiba, H. Kumigashira, "Thickness dependence of electronic structures in VO_2 ultrathin films: Suppression of the cooperative Mott–Peierls transition", *Phys. Rev. B* **102** (2020), article no. 115114.

[153] J. Y. Prieur, P. Seznec, S. Ziolkiewicz, "Temperature variation of the ultrasonic attenuation and phase velocity in VO_2 and V_2O_3 crystals", *J. Phys. (France) Lett.* **38** (1977), p. L25-L28.

[154] T. Lovorn, S. K. Sarker, "Complex quasi-two-dimensional crystalline order embedded in VO_2 and other crystals", *Phys. Rev. Lett.* **119** (2017), article no. 045501.

[155] J. P. Pouget, C. Escribe-Filippini, B. Hennion, R. Currat, A. H. Moudden, R. Moret, J. Marcus, C. Schlenker, "Neutron and X ray studies of the quasi-one-dimensional conductor $K_{0.3}MoO_3$", *Mol. Cryst. Liq. Cryst.* **121** (1985), p. 111-115.

[156] B. Guster, M. Pruneda, P. Ordejón, E. Canadell, J.-P. Pouget, "Evidence for the weak coupling scenario of the Peierls transition in the blue bronze", *Phys. Rev. Mater.* **3** (2019), article no. 055001.

[157] F. Gervais, W. Kress, "Lattice dynamics of oxides with rutile structure and instabilities at the metal-semiconductor phase transitions in VO_2 and NbO_2", *Phys. Rev. B* **31** (1985), p. 4809-4814.

[158] S. Kim, K. Kim, C.-J. Kang, B. I. Min, "Correlation-assisted phonon softening and the orbital-selective Peierls transition in VO_2", *Phys. Rev. B* **87** (2013), article no. 195106.

[159] R. Srivasrava, L. L. Chase, "Raman spectrum of semiconducting and metallic VO_2", *Phys. Rev. Lett.* **27** (1971), p. 727-730.
[160] A. G. Aronov, D. N. Mirliri, I. I. Reshina, F. A. Chudnovskii, "Spectrum of Raman scattering of light and phase transition in VO_2", *Sov. Phys. Solid State* **19** (1977), p. 110-114.
[161] V. S. Vikhnin, N. Goncharuk, V. Y. Davydov, F. A. Chudnovskii, E. B. Shadrin, "Raman spectra of the high-temperature phase of vanadium dioxide and model of structural transformations near the metal-semiconductor phase transition", *Phys. Solid State* **37** (1995), p. 1971-1978.
[162] P. Schilbe, "Raman scattering in VO_2", *Physica B* **316** (2002), p. 600-602.
[163] N. Goncharuk, A. V. Ilinskiy, O. E. Kvashenkina, E. B. Shadrin, "Electron-electron correlations in Raman spectra of VO_2", *Phys. Solid State* **55** (2013), p. 164-174.
[164] J. P. Pouget, B. Hennion, C. Escribe-Filippini, M. Sato, "Neutron-scattering investigations of the Kohn anomaly and of the phase and amplitude charge-density-wave excitations of the blue bronze $K_{0.3}MoO_3$", *Phys. Rev. B* **43** (1991), p. 8421-8430.
[165] R. Pynn, J. D. Axe, P. M. Raccah, "Structural fluctuations in NbO_2 at high temperatures", *Phys. Rev. B* **17** (1978), p. 2196-2205.
[166] L. Lee, K. Hippalgaonkar, F. Yang, J. Hong, C. Ko, J. Suh, K. Liu, K. Wang, J. J. Urban, X. Zhang *et al.*, "Anomalously low electronic thermal conductivity in metallic vanadium dioxide", *Science* **355** (2017), p. 371-374.
[167] R. Comès, M. Lambert, A. Guinier, "The chain structure of $BaTiO_3$ et $KNbO_3$", *Solid State Commun.* **6** (1968), p. 715-719.
[168] H. Takahashi, "A note on the theory of barium titanate", *J. Phys. Soc. Japan* **16** (1961), p. 1685-1689.
[169] S. Ravy, J.-P. Itié, A. Polian, M. Hanfland, "High-pressure study of X-ray diffuse scattering in ferroelectric perovskites", *Phys. Rev. Lett.* **99** (2007), article no. 117601.
[170] J.-P. Pouget, E. Canadell, B. Guster, "Momentum dependent electron-phonon coupling in charge density wave systems", *Phys. Rev. B* **103** (2021), article no. 115135.
[171] P. Foury-Leylekian, J.-P. Pouget, "Peierls transition in two-dimensional metallic monophosphate tungsten Bronzes", *Solid State Sci.* **4** (2002), p. 387-396.
[172] D. Paquet, P. Leroux-Hugon, "Electron correlations and electron-lattice interactions in the metal-insulator, ferroelastic transition in VO_2: A thermodynamical study", *Phys. Rev. B* **22** (1980), p. 5284-5301.
[173] F. Gandi, A. Amaricci, F. Fabrizio, "Unraveling the Mott–Peierls intrigue in Vanadium dioxide", *Phys. Rev. Res.* **2** (2020), article no. 013298.
[174] V. Ilakovac, A. Girard, V. Balédent, P. Foury-Leylekian, B. Winkler, I. Kupčić, H. Berger, A. Bosak, J.-P. Pouget, "Order-disorder type of Peierls instability in $BaVS_3$", *Phys. Rev. B* **103** (2021), article no. 014306.
[175] C. C. Yu, P. W. Anderson, "Local-phonon model of strong electron-phonon interactions in A15 compounds and other strong-coupling superconductors", *Phys. Rev. B* **29** (1984), p. 6165-6186.
[176] P. Y. Le Daeron, S. Aubry, "Metal-insulator transition in incommensurate Peierls chains by extinction of the Frohlich conductivity", *J. Phys. Colloq.* **44** (1983), p. C3-1573-C3-1577.
[177] L. P. Gor'kov, "Strong electron-lattice coupling as the mechanism behind charge density wave transformations in transition-metal dichalcogenides", *Phys. Rev. B* **85** (2012), article no. 165142.
[178] T. A. Mellan, H. Wang, U. Schwingenschlögl, R. Grau-Crespo, "The origin of the transition entropy in vanadium dioxide", *Phys. Rev. B* **99** (2019), article no. 064113.
[179] J. Paras, A. Allanore, "Electronic entropy contribution to the metal insulator transition in VO_2", *Phys. Rev. B* **102** (2020), article no. 165138.
[180] M. Lambert, R. Comès, "The chain structure and phase transition of $BaTiO_3$ and $KNbO_3$", *Solid State Commun.* **7** (1969), p. 305-308.
[181] J. P. Pouget, P. Alemany, E. Canadell, "Donor–anion interactions in quarter-filled low-dimensional organic conductors", *Mater. Horiz.* **5** (2018), p. 590-640.
[182] P. Alemany, J. P. Pouget, E. Canadell, "Structural and electronic control of the metal to insulator transition and local orderings in the θ-(BEDT-TTF)2X organic conductors", *J. Phys.: Condens. Matter* **27** (2015), article no. 465702.
[183] M. Liu, A. J. Sternbach, A. J. Basov, "Nanoscale electrodynamics of strongly correlated quantum materials", *Rep. Prog. Phys.* **80** (2017), article no. 014501.
[184] Y. Zhu, Z. Cai, P. Chen, Q. Zhang, M. J. Highland, I. W. Jung, D. A. Walko *et al.*, "Mesoscopic structural phase progression in photo-excited VO_2 revealed by time-resolved x-ray diffraction microscopy", *Sci. Rep.* **6** (2016), article no. 21999.
[185] T. L. Cocker, L. V. Titova, S. Fourmaux, G. Holloway, H.-C. Bandulet, D. Brassard *et al.*, "Phase diagram of the ultrafast photoinduced insulator-metal transition in vanadium dioxide", *Phys. Rev. B* **85** (2012), article no. 155120.
[186] A. Cavalleri, D. Th., H. H. Chong, J. C. Kieffer, R. W. Schoenlein, "Evidence for a structurally-driven insulator-to-metal transition in VO_2: a view from the ultrafast timescale", *Phys. Rev. B* **70** (2004), article no. 161102(R).
[187] C. Kübler, H. Ehrke, R. Huber, R. Lopez, A. Halabica, R. F. Haglund Jr, A. Leitenstorfer, "Coherent structural dynamics

and electronic correlations during an ultrafast insulator-to-metal phase transition in VO_2", *Phys. Rev. Lett.* **99** (2007), article no. 116401.

[188] H.-T. Kim, Y. W. Lee, B.-J. Kim, B.-G. Chae, S. J. Yun, K.-Y. Kang, K.-J. Han *et al.*, "Monoclinic and correlated metal phase in VO_2 as evidence of the Mott transition: coherent phonon analysis", *Phys. Rev. Lett.* **97** (2006), article no. 266401.

[189] Z. Tao, F. Zhou, T.-R. T. Han, D. Torres, T. Wang, N. Sepulveda, K. Chang, M. Young, R. R. Lunt, C.-Y. Ruan, "The nature of photoinduced phase transition and metastable states in vanadium dioxide", *Sci. Rep.* **6** (2016), article no. 38514.

[190] T. V. Slusar, J.-C. Cho, H.-R. Lee, J.-W. Kim, S. J. Yoo *et al.*, "Mott transition in chain structure of strained VO_2 films revealed by coherent phonons", *Sci. Rep.* **7** (2017), article no. 16038.

[191] T. Soma, T. Kobayashi, K. Yoshimatsu, A. Ohtomo, "Superconducting dome underlying bipolaronic insulating state in charge doped Ti_4O_7 epitaxial films", *J. Phys. Soc. Japan* **90** (2021), article no. 023705.